Applied Thermal Engineering 294 (2026) 130568

Contents lists available at ScienceDirect

Applied Thermal Engineering

journal homepage: www.elsevier.com/locate/apthermeng

Research Paper

A combined thermal-resistance-capacity and finite-element model for the short- and medium-term simulation of single U-tube borehole heat exchangers

Enzo Zanchini [a,*], Francesco Zanchini [b], Claudia Naldi [a]

[a] Department of Industrial Engineering, Viale del Risorgimento 2, University of Bologna, Bologna, Italy
[b] Student of the Department of Physics and Astronomy, Viale Carlo Berti Pichat 6/2, University of Bologna, Bologna, Italy

ARTICLE INFO

Keywords:
Borehole heat exchangers
Short-term simulation
Medium-term simulation
Thermal resistance capacity model

ABSTRACT

An accurate design of a ground-coupled heat pump system requires the knowledge of the outlet fluid temperature from the borehole heat exchangers (BHEs), both in the short and long term. This paper focuses on the short and medium term. In this time range, either 3D finite-element simulations or Thermal Resistance Capacity Models (TRCMs) can be applied. The former can yield very accurate results but require long computation times. The latter are much faster but cannot be fully precise, because they require simplifying assumptions. In this paper, we present a new method for the short-term and medium-term simulation of single U-tube BHEs, which combines the speed of TRCMs and the accuracy of finite-element simulations. The method uses a TRCM to estimate the thermal response of the BHE, then corrects the results by interpolation with a dataset, which has been produced by running 54 finite-element simulations in various configurations. The model is implemented in a C++ program, available at the open-source online data repository of the University of Bologna. The program provides, within two seconds, the time evolution of the inlet, outlet and mean fluid temperature, of the mean BHE surface temperature, of the 3D and the effective borehole thermal resistance. It can be easily connected to long-term simulation tools to obtain the full-time-scale thermal response of a bore field.

1. Introduction

Ground-coupled heat pumps are very efficient systems for heating and cooling buildings. Usually, the heat exchange with the ground is obtained by means of vertical ground heat exchangers, called Borehole Heat Exchangers (BHEs), composed of either a single U-tube or a double U-tube in high density polyethylene, surrounded by a sealing grout.

An accurate design of a ground-coupled heat pump system requires the knowledge of the time evolution of the fluid temperature at the outlet of the bore field, T_{out}, both in the short and long term. This thermal response is usually determined by employing a dimensionless function, called *g-function*, which yields the time evolution of the mean temperature of the surface between the BHEs and the ground, T_b, due to a time constant heat load. The time evolution of T_b produced by a time dependent heat load is then obtained by the superposition of the effects in time.

Once the *g-function* has been obtained, one needs to determine the time evolution of T_{out} starting from that of T_b. This is done through either the mean fluid temperature, T_{fm}, or the arithmetic mean of inlet and outlet fluid temperature, $T_{fave} = (T_{in} + T_{out})/2$. The mean fluid temperature can be deduced from T_b by the relation

$$T_{fm} = T_b + \dot{q}_l R_{b3D}, \tag{1}$$

where $\dot{q}_l$ is the mean heat rate per unit length supplied to the bore field, and R_{b3D} is the 3D borehole thermal resistance, usually assumed as coincident with the 2D thermal resistance of a BHE cross section, R_b. The time evolution of T_{fave} can be deduced from that of T_b by the relation

$$T_{fave} = T_b + \dot{q}_l R_{beff}, \tag{2}$$

where R_{beff} is the effective borehole thermal resistance. Accurate analytical expressions for R_b and for R_{beff} are now available in the literature, but these expressions hold for quasi-stationary heat transfer inside the BHE. Thus, the time evolution of T_{out} in transient regime cannot be determined accurately by means of Eqs. (1) and (2) and the available analytical expressions of R_b and R_{beff}.

In transient conditions, namely soon after the start of the BHE

* Corresponding author.
E-mail address: enzo.zanchini@unibo.it (E. Zanchini).

https://doi.org/10.1016/j.applthermaleng.2026.130568
Received 27 October 2025; Received in revised form 6 March 2026; Accepted 8 March 2026
Available online 15 March 2026

Nomenclature

ANN	Artificial neural network
b	Borehole node
BHE	Borehole Heat Exchanger
c	Specific heat capacity $\left(\mathrm{J\,kg^{-1}K^{-1}}\right)$
c_{coeff}	Correction coefficient, defined in Eq. (29)
C	Heat capacity $\left(\mathrm{J\,K^{-1}}\right)$
D	Buried depth (m)
f	Weighting factor, defined in Eq. (4)
$\mathrm{f}_1, \mathrm{f}_2$	downward and upward fluid nodes
FLS	Finite line-source
g_i	i-th ground node, $i = 1, 2, \ldots, n+1$
gt_1, gt_2	grout nodes
h	Convection coefficient $\left(\mathrm{W\,m^{-2}K^{-1}}\right)$
HUST	Horizontally uniform surface temperature
k	Thermal conductivity $\left(\mathrm{W\,m^{-1}K^{-1}}\right)$
l	Height of each horizontal slice (m)
L	BHE height (m)
m	Number of horizontal slices
$\dot{m}_{\mathrm{f}}$	Mass flow rate of the fluid $\left(\mathrm{kg\,s^{-1}}\right)$
n	Number of ground annuli
Nu	Nusselt number
p_1, p_2	pipe nodes
$\dot{q}_{\mathrm{l}}$	Mean heat rate per unit length $\left(\mathrm{W\,m^{-1}}\right)$
$\dot{Q}$	Heat rate supplied to the BHE (W)
r_0, r_{b}	BHE radius (m)
r_i	Radius of the outer surface of the i-th ground annulus (m)
$\bar{r}_i$	Radius defined in Eq. (13) (m)
RMSD	Root mean square difference
r_{pe}	Outer radius of the pipe (m)
r_{pi}	Inner radius of the pipe (m)
r_x	Radial distance from the BHE axis, defined in (Ruiz-Calvo et al., 2015) (m)
R_1^{Δ}	Thermal resistance per unit length between fluid 1 and the BHE wall $\left(\mathrm{m\,K\,W^{-1}}\right)$
R_2^{Δ}	Thermal resistance per unit length between fluid 2 and the BHE wall $\left(\mathrm{m\,K\,W^{-1}}\right)$
R_{12}^{Δ}	Thermal resistance per unit length between fluid 1 and fluid 2 $\left(\mathrm{m\,K\,W^{-1}}\right)$
R_{a}	Total thermal resistance per unit length between the flows, $\left(\mathrm{m\,K\,W^{-1}}\right)$
R_{b}	2D steady-state borehole thermal resistance per unit length $\left(\mathrm{m\,K\,W^{-1}}\right)$
R_{b3D}	3D borehole thermal resistance per unit length $\left(\mathrm{m\,K\,W^{-1}}\right)$
R_{beff}	Effective borehole thermal resistance per unit length $\left(\mathrm{m\,K\,W^{-1}}\right)$
R_{conv}	Convective thermal resistance per unit length $\left(\mathrm{m\,K\,W^{-1}}\right)$
R_i	Thermal resistance per unit length of the ground between $\bar{r}_{i-1}$ and $\bar{r}_i$ $\left(\mathrm{K\,W^{-1}}\right)$
s	Half shank spacing (m)
t	Time (s)
t^*	Dimensionless time, defined in Eq. (8)
T	Temperature $(^\circ\mathrm{C})$
T_{b}	Mean temperature of the BHE surface $(^\circ\mathrm{C})$
T_{fave}	$= (T_{\mathrm{in}} + T_{\mathrm{out}})/2$ $(^\circ\mathrm{C})$
T_{fm}	Mean temperature of the fluid $(^\circ\mathrm{C})$
T_{g}	Undisturbed ground temperature $(^\circ\mathrm{C})$
T_{in}	Inlet fluid temperature $(^\circ\mathrm{C})$
T_{out}	Outlet fluid temperature $(^\circ\mathrm{C})$
TRCM	Thermal Resistance Capacity Model
TRT	Thermal response test
$\dot{V}$	Volume flow rate $\left(\mathrm{m^3 s^{-1}}\right)$
$\dot{V}_0$	Reference volume flow rate $\left(\mathrm{m^3 s^{-1}}\right)$

Subscripts

0	Reference, initial, of the borehole node
c	Corrected
f	Of fluid
f1, f2	Of the fluid node f_1, of the fluid node f_2
g	Of ground
gt	Of grout
gt1, gt2	Of the grout node gt_1, of the grout node gt_2
i	Of the i-th ground annulus, of the i-th ground node, $i = 1, 2, \ldots, n+1$
j	Of the j-th horizontal slice, $j = 1, 2, \ldots, m$
k	Of the k-th time instant, $k = 1, 2, \ldots K$
p	Of pipe
p1, p2	Of the pipe node p_1, of the pipe node p_2

Greek symbols

ε	Fraction of the grout heat capacity placed in the grout nodes
η	Dimensionless parameter, defined in Eq. (7)
ρ	Density $\left(\mathrm{kg\,m^{-3}}\right)$
(ρc)	Volumetric heat capacity $\left(\mathrm{J\,m^{-3}K^{-1}}\right)$
φ	Dimensionless coefficient, defined in Eq. (5)

operation or a sudden change in heat load, the time-dependent values of R_{b3D} and of R_{beff} differ considerably from the quasi-stationary values. As a consequence, it is necessary to perform an accurate short-term simulation of the BHE, to obtain the correct time evolution of T_{out}. The short-term simulation can be performed using an analytical solution, a 3D numerical simulation, or a lumped-parameter model.

Relevant contributions to the evaluation of the *g-function* of a bore field, to the methods to determine the time evolution of T_{out} starting from that of T_{b}, and to the short-term simulation of a BHE are recalled below.

1.1. Evaluation of the g-function

The simplest way to determine the *g-function* of a bore field is to use the finite line-source (FLS) model with uniform heat load. This condition allows determining the *g-function* of the bore field using the analytical expression of the temperature field around a single BHE [1] and the superposition of the effects in space. However, the FLS model with uniform heat load yields an overestimation of the *g-function* of the bore field, that can be relevant for large and compact bore fields [2– 4].

A more accurate FLS model is the one proposed by Eskilson [5], in which the condition of uniform heat load is replaced by that of uniform surface temperature of the bore field. A semi-analytical method to determine *g-functions* of bore fields with Eskilson's boundary condition was developed by Cimmino and Bernier [6], and numerical methods were proposed by Monzó et al. [7] and by Naldi and Zanchini [8].

The condition of uniform surface temperature yields a slight underestimation of the *g-function* of a bore field [9]. A semi-analytical model that employs the real condition of BHEs fed in parallel with the same inlet temperature was developed by Cimmino [9]: each borehole is divided into segments having uniform temperature and heat rate, and is modeled as a finite line source. Improvements of the model, aimed to

reduce the computation time were proposed in [10 –12]. Numerical models using the condition of uniform fluid temperature were proposed by Monzó et al. [13] and by Zanchini et al. [14], and a semi-analytical model with this condition was developed by E. Zanchini and F. Zanchini [15]. For U-tube BHEs, the condition of uniform fluid temperature yields the same *g-function* as the condition of BHEs fed in parallel with the same inlet temperature [16]. Recently, Cimmino et al. [17] presented a major improvement of the model proposed in [9], by considering polynomial variations of temperature and heat rate along each segment. The new model enables the simulation of boreholes with curved trajectories.

1.2. Calculation of T_{out} starting from T_b

The first step to determine the time evolution of T_{out} starting from that of T_b is determining the time evolution of T_{fm}, through R_{b3D} and Eq. (1), or that of T_{fave}, through R_{beff} and Eq. (2).

A pioneering contribution to this goal was made by Hellström [18], who illustrated a general method for deriving expressions of the thermal resistances of BHEs, and provided an expression of R_b for single U-tube BHEs, based on the line-source approximation. He also proposed a relation for determining R_{beff} from R_b, and illustrated how to perform more accurate calculations of thermal resistances by the multipole method. More recently, Javed and Spitler [19] proposed very accurate first-order multipole expressions of R_b and of the total internal resistance between the pipes, R_a. Claesson and Javed [20] determined first-order multipole expressions of R_b and R_a for double U-tube BHEs, and extended to these BHEs Hellström's relation between R_{beff} from R_b.

When the time evolution of T_{fave} has been found, that of T_{out} is given by

$$T_{out} = T_{fave} - 0.5\frac{\dot{Q}}{\dot{m}_f c_f}, \tag{3}$$

where $\dot{Q}$ is the mean heat rate supplied to each BHE, $\dot{m}_f$ is the mass flow rate circulating in each BHEs, c_f is the specific heat capacity at constant pressure of the fluid.

The outlet fluid temperature can also be obtained from T_{fm} through the equation proposed by Beier and Spitler [21], namely

$$T_{out} = T_{fm} - f\frac{\dot{Q}}{\dot{m}_f c_f}, \tag{4}$$

where f is a weighting factor that can be determined as described in [21]. As an alternative, T_{out} can be obtained from T_{fm} through the equation proposed by Jahanbin et al. [22], namely

$$T_{out} = T_{fm} - \left(0.5 - \varphi\frac{\dot{V}}{\dot{V}_0}\right)\frac{\dot{Q}}{\dot{m}_f c_f}, \tag{5}$$

where $\dot{V}$ is the fluid volume flow rate in each BHE, $\dot{V}_0$ is a reference volume flow rate, equal to 12 l per minute, and φ is a dimensionless coefficient that can be determined by the correlations given in Jahanbin et al. [22] for single U-tube BHEs and in Zanchini and Jahanbin [23] for double U-tube BHEs.

Thus, the problem of determining T_{out} from T_b in quasi-stationary conditions can be considered as solved, even if the quasi-stationary value of R_{b3D} is slightly greater than R_b [16], and the quasi-stationary value of R_{beff} is slightly greater than that given by Hellström's method, as is shown in this paper.

On the contrary, the problem of determining the time evolution of T_{out} soon after the start of the BHE operation or a sudden change in heat load requires a short-term simulation program.

1.3. Short-term simulation of a BHE

The short-term simulation of a BHE can be performed using an analytical solution, a 3D numerical simulation, or a lumped-parameter model.

Analytical solutions of short-term BHE models where the fluid is replaced by a heat generating solid, or surface, or set of lines, have been proposed by Lamarche and Beauchamp [24], Bandyopadhyay et al. [25,26], Man et al. [27], Li and Lay [28], Lamarche [29]. These models, even if accurate, cannot take into account the effects of the heat exchange between the descending and the ascending flow, which enhances R_{b3D} and, as a consequence, T_{fm} [16].

An analytical short-term model of single U-tube BHEs that considers the energy balances along the flow has been developed by Beier [30]. In the model, the pipes are replaced by two adjacent half pipes separated by a thermal resistance and surrounded by the grout. The solution is given in the Laplace transformed domain and requires a numerical inverse Laplace transform algorithm. Recently, Beier [31] developed an explicit analytical solution of the heat transfer in a U tube BHE, which holds in the presence of a uniform geothermal gradient. Although the solution assumes a quasi-stationary regime within the BHE, it is a useful tool for evaluating the effect of the geothermal gradient on thermal response tests (TRTs).

Numerical 3D simulations of U-tube BHEs considering the energy balance along the flow have been performed by several authors. Li and Zheng [32], Florides et al. [33], Ozudogru et al. [34], Lei et al. [35], and Zanchini [16] proposed models with 3D simulation of the solid domain and 1D energy balance along the flow. Marcotte and Pasquier [36] and Pasquier and Marcotte [37] employed models with the 3D simulation of both the solid and the fluid domain, with a uniform velocity of the fluid. A 3D simulation can yield very accurate results, but requires a long computation time, typically several hours for each simulation.

As an alternative to numerical simulations that solve the local energy balance equations, some authors developed lumped-parameters numerical models based on the electric analogy, where the BHE and the ground are represented by a grid of thermal resistances and heat capacities.

De Carli et al. [38] developed a 3D Capacity Resistance model where the BHE and the ground are divided into m horizontal slices, and the ground is divided into n coaxial cylindrical regions. The conduction heat transfer is assumed to occur only in the radial direction, and the energy transfer in the vertical direction is due to the fluid flow. While both thermal resistances and heat capacities are considered for the ground elements, the heat capacity of the borehole is neglected. Zarrella et al. [39] developed an improved model, in which the heat capacities of both the sealing grout and the heat carrier fluid are considered. The model refers to double U-tube BHEs. The grout is divided into a core region, between the pipes, and a shell region, from the pipes to the borehole wall.

Bauer et al. [40] developed 2D Thermal Resistance Capacity Models (TRCMs) for coaxial, single U-tube, and double U-tube BHEs. The model for single U-tube BHEs is composed of two fluid nodes without heat capacities, two grout nodes, each with heat capacity equal to one half of the heat capacity of the grout, one borehole node without heat capacity, and several ground nodes. The thermal short circuiting between the pipes is considered by means of a grout-to-grout thermal resistance.

Bauer et al. [41] developed a 3D TRCM for single U-tube BHEs based on the 2D horizontal thermal circuit proposed in Bauer et al. [40]. In the new 3D model, the fluid nodes have the heat capacity of the corresponding fluid, and the horizontal thermal circuits are connected in the vertical direction by considering the heat transfer between overlapping nodes and the mass transport in the fluid. A validation of the model revealed a fair agreement between the outlet temperature of the fluid yielded by the model and that yielded by a finite-element simulation.

Pasquier and Marcotte [42] proposed an improvement of the 2D model by Bauer et al. [40], where each node is split in several nodes, and the grout thermal resistance and the grout-to-grout thermal resistance are split in several equal parts in series. The same authors [37] transformed the 2D model of [42] into a quasi 3D model considering the

Table 1
Geometrical and thermal parameters of the BHEs employed in the examples.

Quantity	Symbol	Unit	BHE 1	BHE 2	BHE3
BHE length	L	m	100	200	80
BHE radius	r_b	mm	76	74	64
Buried depth	D	m	1.8	1.8	1.8
Half shank spacing	s	mm	47	40	32
Pipe outer radius	r_{pe}	mm	20	20	16
Pipe inner radius	r_{pi}	mm	16.3	16.3	13
Pipe thermal conductivity	k_p	W/(m K)	0.4	0.4	0.4
Pipe volumetric heat capacity	$(\rho c)_p$	MJ/(m^{3}K)	1.824	1.824	1.824
Grout thermal conductivity	k_{gt}	W/(m K)	1.0	1.8	2.0
Grout volumetric heat capacity	$(\rho c)_{gt}$	MJ/(m^{3}K)	2.5	2.3	2.8
Ground thermal conductivity	k_g	W/(m K)	1.8	1.6	1.2
Ground volumetric heat capacity	$(\rho c)_g$	MJ/(m^{3}K)	2.8	3.0	2.2
Volume flow rate	$\dot{V}$	liters/min	14	22	12
Mean heat rate per unit length	$\dot{q}_l$	W/m	50	50	50

vertical energy transfer by the fluid, and validated the new model by comparing its outcomes with those of a 3D finite-element model and with the experimental results of two TRTs.

Ruiz-Calvo et al. [43] developed a lumped-parameter model called Borehole-to-Ground where a vertical discretization of the BHE and the soil is introduced, and five nodes are considered for each depth: two fluid nodes, two grout nodes and one ground node. Each grout node has half of the heat capacity of the grout and is placed at a radial distance r_x from the BHE axis, to be optimized. Each fluid node is connected to the ground node by four thermal resistances in series, whose expressions are given by Eqs. (13), (16), (17), and (21) of [43]. The thermal interference between the descending and the ascending flow is considered by means of a pipe-to-pipe and a grout-to-grout thermal resistance, given by Eqs. (18) and (19) of [43]. The model has no borehole node. This way, the authors avoided the assumption of an isothermal surface of the BHE, but were forced to use approximate expressions for the thermal resistances. Since the model employs only one ground node, it becomes inaccurate when the simulation period exceeds 18 h.

Pasquier et al. [44] developed an artificial neural network (ANN) that constructs very rapidly both the short-term and the long-term thermal response of a field of single U-tube BHEs. The short-term thermal response is based upon a training set of 15,000 simulations performed with the TRCM of [37]. The ANN allows only one value of the inner and of the outer radius of the pipes and considers a vanishing convective thermal resistance between fluid and pipes. The MATLAB code of the ANN is available as supplementary material of the paper. Pasquier and Marcotte [45] extended the ANN to other values of the inner and outer radius of the pipes and to a larger set of allowed input parameters, still with a vanishing convective thermal resistance between fluid and pipes.

Most TRCMs assume a horizontally uniform surface temperature (HUST) of the BHE [37–42,44,45]. This assumption is necessary in order to use the accurate analytical expressions of the thermal resistances between each pipe and the borehole wall and between the pipes determined by the multipole method [19,20]. However, as we will show in Section 2, the HUST condition yields an underestimation of R_{b3D} which, in turn, yields an underestimation of T_{fm}, T_{in}, and T_{out}. The underestimation becomes appreciable after a few hours of operation.

In this paper we propose a new method for the short-term and medium-term simulation of single U-tube BHEs. The method is based on a TRCM, where the BHE and the ground are divided into horizontal slices, each modeled with a thermal circuit. The inaccuracies of the TRCM are corrected through a dataset of correction factors. The dataset has been produced by comparing the time evolution of R_{b3D} yielded by the TRCM with that obtained by a very accurate 3D finite-element simulation in 54 different configurations. The correction factors in the remaining configurations are obtained by applying polynomial interpolation techniques to the dataset. The method has been implemented in a C++ program that yields, within two seconds, the same time evolution of T_b, T_{fm}, T_{in}, T_{out}, R_{b3D}, and R_{beff} that can be obtained by a finite-element simulation requiring several computation hours. The C++ program is available at the open-source online data repository of the University of Bologna (see data availability).

The application of the correction factors makes the proposed model much more accurate than the existing TRCMs. Due to its high speed and accuracy, the model is particularly suitable for the numerical evaluation of TRTs. The model can also provide time dependent values of R_{b3D} and R_{beff} to be used in programs for the long-term simulation of bore fields subjected to a time-constant heat load. This way, long term simulation models can be transformed into models valid over the whole time scale.

The paper is organized as follows. In Section 2, we describe our 3D finite-element simulation model and we use it to show that the HUST condition yields an underestimation of the thermal response. In Section 3, we describe the proposed TRCM. In Section 4, we compare the results of the TRCM with those of the finite-element model, we highlight the inaccuracies of the TRCM, and we point out that they can only be corrected a posteriori. In Section 5, we show that the inaccuracies can be resolved by introducing a time-dependent correction factor. In Section 6, we illustrate the results of the corrected TRCM. In Section 7, we validate both the COMSOL model and the TRCM by reproducing the time evolution of T_{in} and T_{out} in a TRT.

2. Description of the finite-element model and effect of the HUST condition

The 3D finite-element simulation model employed in [16] was selected for the 3D simulations of this paper. The model was chosen due to its accuracy, demonstrated in [16] through mesh-independence tests and through the comparison with the FLS solution of Claesson and Javed [1] in a special case.

The model employs the Heat Transfer in Solids interface of COMSOL Multiphysics to simulate the heat conduction in the solid domains, and the COMSOL Pipe Flow Module to simulate the energy balance along the flow. The module is implemented with the method recommended in [16].

The fluid, represented by a line, flows in a closed circuit, and a heat generation is placed in the upper connection between the flows. For all simulations, the fluid considered is water, with thermal properties at 20 °C, taken from the NIST Chemistry WebBook [46]: density 998.21 kg/m^3, dynamic viscosity 1.0016 mPa s, thermal conductivity 0.59801 W/(m K), specific heat capacity at constant pressure 4.1841 kJ/(kg K). The convection coefficient, h, is determined through the Nusselt number, Nu, calculated by the Churchill correlation [47].

The pipes are represented by solid cylinders having the same thermal conductivity as the real pipes, and a reduced volumetric heat capacity, given by $0.5(\rho c)_p\left(r_{pe}^2 - r_{pi}^2\right)/r_{pe}^2$, as in [16]. This is to eliminate the overestimation of the heat capacity of the pipes due to considering solid pipes instead of the real annular ones.

In all simulations, except those of Section 7, the BHE is interred at a buried depth $D = 1.8$ m. The selected computational domain is a cylinder with radius 100 m and height 101.8 m greater than the BHE length, with the vertical axis oriented upwards and origin at the BHE top. The ground surface is considered as isothermal, with temperature $T_g = 0$ °C, equal to the undisturbed ground temperature and to the initial temperature. The vertical and the bottom surfaces of the computational domain are set to adiabatic. Although the radius of the computational domain could have been reduced, the same radius as in [16] was preferred, to use the meshes adopted in [16] as a reference.

To ensure high accuracy, the results are collected starting from 10^{-4}

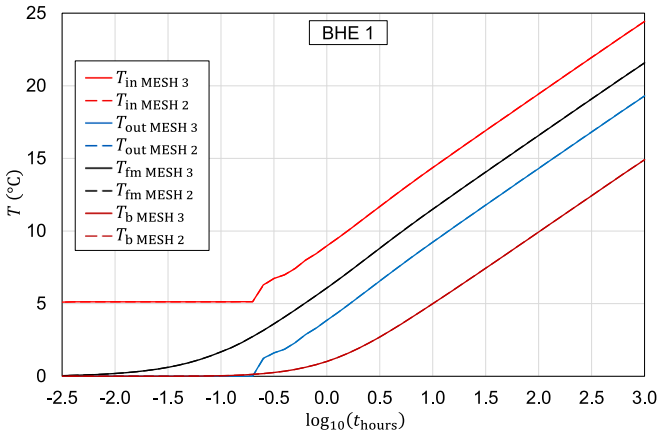

Fig. 1. Time evolutions of T_{in}, T_{out}, T_{fm} and T_b for BHE 1, obtained by Mesh 2 and Mesh 3.

hours, the initial step is set to 10^{-6} hours, and the absolute accuracy is set to 10^{-4}. To improve meshing, the lengths in the vertical direction are reduced by a scaling factor 20, and the thermal conductivities of the solids in the vertical direction are reduced by a scaling factor 400. The thermal conductivity of water, which is a scalar in the Pipe Flow Module, is reduced by the factor 400, and the Nusselt number is multiplied by 400.

The mesh used for the simulations is intermediate between Mesh 1 and Mesh 2 employed in [16]. This intermediate mesh, which will be denoted by Mesh 3, provides almost identical results to Mesh 2, but allows for a reduction in computation time. It is obtained by setting minimum element size 2 mm, maximum element size 4 m, element growth rate 1.25, curvature factor 1.

The U-tube BHE considered in this section will be denoted by BHE 1. It has length $L = 100$ m, radius $r_b = 76$ mm, half shank spacing $s = 47$ mm, and is placed in a ground with thermal conductivity $k_g = 1.8$ W/(m K). The volume flow rate of the fluid is 14 l per minute, and the heat rate released to the fluid corresponds to a mean heat rate per unit length $\dot{q}_l = 50$ W/m. The parameters that characterize BHE 1 are summarized in Table 1, fourth column. For BHE 1, one has $Nu = 80.2108$, $h = 1471.4\ \mathrm{W/(m^2K)}$.

The mesh independence of the results for BHE 1 is illustrated in Fig. 1, where the time evolutions of T_{in}, T_{out}, T_{fm}, and T_b obtained with Mesh 3, having 575,860 elements, are compared with those obtained with Mesh 2, having 949,178 elements. The results are reported at 56 time instants, equally spaced in a logarithmic scale from $10^{-2.5}$ hours (about 11.4 s) to 10^3 hours. The root mean square difference (RMSD) between the results obtained with the two meshes is 0.007 °C for T_{in} and T_{fm}, 0.008 °C for T_{out}, and 0.002 °C for T_b. A very steep increase of T_{in} and T_{out} occurs after $\log_{10}(t_{hours}) = -0.7$, i.e. $t = 11.97$ minutes, namely 1.54 min after the completion of the circuit by the heated fluid. Before that instant, T_{in} and T_{out} remain constant.

In order to determine the errors due to the HUST condition, we performed an additional simulation of BHE 1, where this condition is forced. In this simulation, a ground cylinder with thickness 4 mm, adjacent to the BHE surface, is replaced by a layer having thermal conductivity 10^6 W/(m K) in the horizontal directions, zero in the vertical direction, and the same volumetric heat capacity as the ground. A thin resistive layer with thickness 0.1 mm and thermal resistance per unit length 0.004535 m K/W is inserted after the high-conductivity layer, to restore the real thermal resistance of the ground. The complete meshed domain and a particular of the mesh at the BHE top are illustrated in Fig. 2. The mesh consists of 654,145 tetrahedral elements. The flat shape of the computational domain is due to the rescaling of the vertical coordinate.

The time evolutions of T_{in}, T_{out}, T_{fm}, and T_b obtained in the real conditions have been compared with those obtained in the simulation with the high-conductivity layer, as illustrated in Fig. 3.

The comparison shows that the HUST condition yields an underestimation of T_{in}, T_{out}, and T_{fm}, while it has no appreciable effect on T_b. The underestimation of T_{fm} is slightly greater than that of T_{in} and T_{out}.

The effect of the high-conductivity layer on R_{b3D} and R_{beff} is illustrated in Fig. 4.

The figure shows that the HUST condition yields an underestimation of R_{b3D} and R_{beff}, and that the underestimation of R_{b3D} is greater than that of R_{beff}. The asymptotic value of R_{beff} obtained in the case of the HUST condition is nearly coincident with the stationary value of R_{beff} given by Hellström's eq. [18],

$$R_{beff} = \eta \coth(\eta)\, R_b, \tag{6}$$

where η is the dimensionless parameter

$$\eta = \frac{L}{\dot{m}_f c_f} \frac{1}{\sqrt{R_a R_b}}, \tag{7}$$

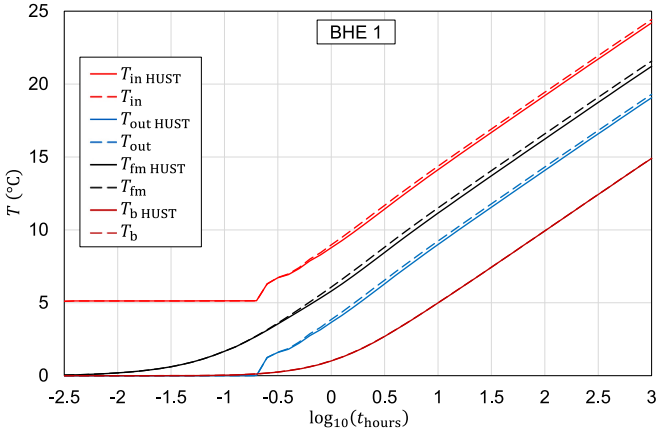

Fig. 3. Time evolutions of T_{in}, T_{out}, T_{fm}, and T_b for BHE 1, in the case of horizontally uniform surface temperature (HUST) of the BHE and in the real case.

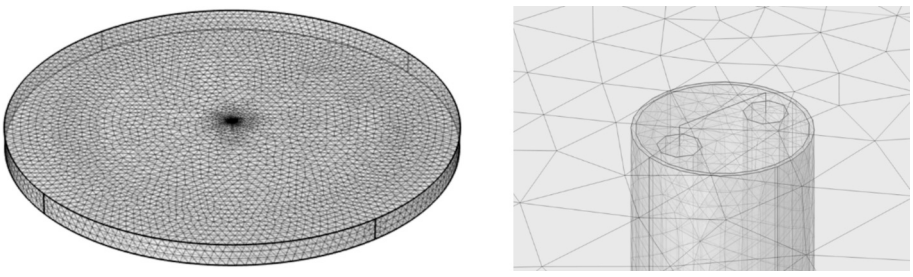

Fig. 2. Mesh employed in the simulation of BHE 1 with the high-conductivity layer: complete meshed domain (left) and particular at the BHE top (right).

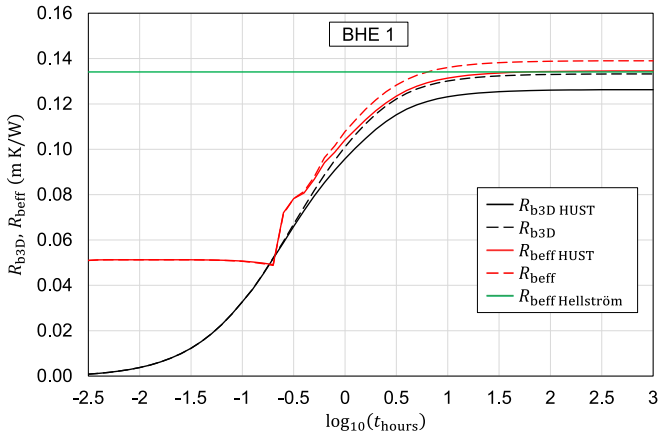

Fig. 4. Time evolutions of R_{b3D} and R_{eff} for BHE 1, in the case of horizontally uniform surface temperature (HUST) of the BHE and in the real case. The green line is the effective borehole thermal resistance given by Hellström's equation. (For interpretation of the references to colour in this figure legend, the reader is referred to the web version of this article.)

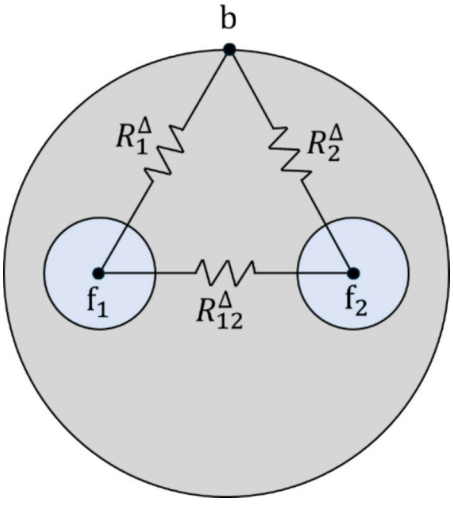

Fig. 5. Standard triangular network of thermal resistances: R_1^Δ is the thermal resistance between fluid 1 and the borehole wall, R_2^Δ is the thermal resistance between fluid 2 and the borehole wall, and R_{12}^Δ is the thermal resistance between the flows.

and R_a is the total thermal resistance per unit length between the descending and the ascending flow.

In summary, the simulation with the high-conductivity layer shows that the HUST condition yields an underestimation of T_{in}, T_{out}, T_{fm}, R_{b3D} and R_{beff}, while it has a negligible effect on T_b. This suggests that the HUST condition may have the same effect on the results of TRCMs.

3. Description of the proposed TRCM

In the proposed TRCM, the BHE and the ground are divided into m horizontal slices of the same height l. Vertical heat conduction in the solid is neglected, so the vertical energy transfer is due only to the fluid flow. For this reason, the model is not suitable for long-term simulations, as vertical heat transfer in the soil becomes significant in the long term. The time limit of validity of the model increases with the BHE length. We performed our simulations for a time period of 1000 h, because this is the longest time that ensures good accuracy for all BHEs longer than 60 m. This limit has been determined by comparing the results given by the model with those from COMSOL Multiphysics. For BHEs with length

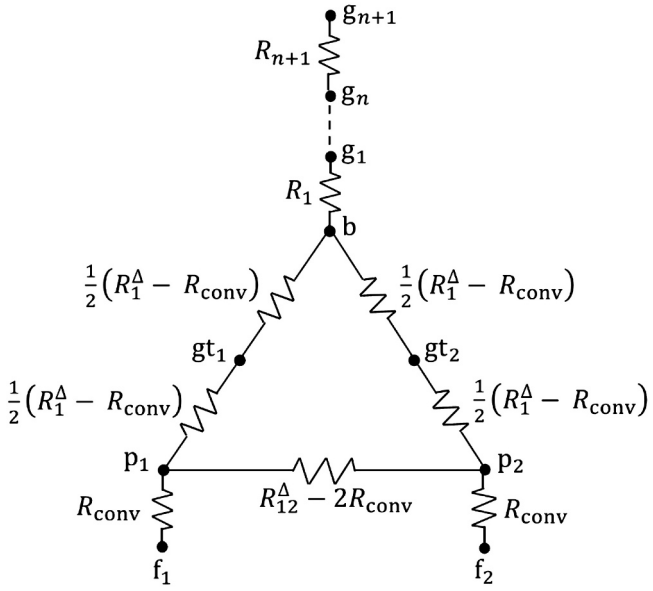

Fig. 6. Network of thermal resistances of the proposed model, for each horizontal slice.

between 40 and 60 m, the model yields accurate results for values of the dimensionless time up to 0.002, with dimensionless time defined as

$$t^* = \frac{9k_g t}{(\rho c)_g L^2}\,. \tag{8}$$

For $L = 40$ m, the time limit is 165 h if $k_g/(\rho c)_g = 6 \times 10^{-7}\mathrm{m}^2/\mathrm{s}$, and 99 h if $k_g/(\rho c)_g = 10^{-6}\mathrm{m}^2/\mathrm{s}$. These limits are sufficient for the numerical evaluation of TRTs.

Each horizontal slice is modeled with a thermal circuit based on the standard triangular network of thermal resistances [18], to which additional nodes are added.

The standard triangular network consists of three nodes: f_1, which represents the downward flow of the fluid, f_2, which represents the upward flow, and b, which represents the external surface of the BHE. The nodes are connected by the thermal resistances per unit length R_1^Δ, R_2^Δ, R_{12}^Δ, as illustrated in Fig. 5. Node f_1 exchanges heat with b through the thermal resistance R_1^Δ, f_2 exchanges heat with b through the thermal resistance R_2^Δ, and f_1 exchanges heat with f_2 through the thermal resistance R_{12}^Δ.

This paper only deals with symmetric pipes, for which $R_2^\Delta = R_1^\Delta$. In this case, the thermal resistances R_1^Δ and R_{12}^Δ can be easily obtained from the borehole thermal resistance, R_b, and the total thermal resistance between the flows, R_a, by the following equations:

$$R_1^\Delta = 2R_b, \tag{9}$$

$$R_{12}^\Delta = \frac{4R_bR_a}{4R_b - R_a}. \tag{10}$$

The values of R_b and R_a used in our simulations have been obtained from the first-order multipole expressions given by Javes and Spitler [19].

In our model, several nodes are added to the standard triangular network. Four nodes are added to better describe the internal structure of the BHE: p_1, representing pipe 1, p_2, representing pipe 2, gt_1, which represents a portion of grout surrounding pipe 1, and gt_2, which represents a portion of grout surrounding pipe 2. The ground is divided into n concentric annuli, each modeled with a node: $g_1, \ldots, g_n$. Finally, one last node, g_{n+1}, is added to represent the unperturbed ground. A diagram of the thermal circuit is shown in Fig. 6.

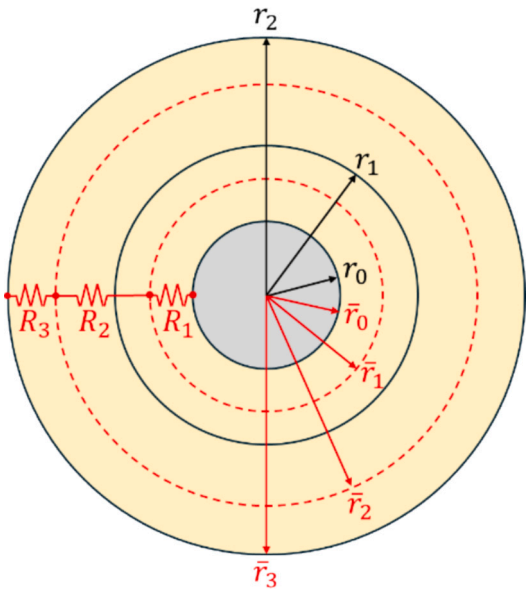

Fig. 7. Partition of the ground in the case of two concentric annuli.

For simplicity, the mass of the pipes is assumed to be concentrated at their inner surface. Therefore, the thermal resistance between f_1 and p_1 (as well as the thermal resistance between f_2 and p_2) is

$$R_{\rm conv} = \frac{1}{2\pi r_{\rm pi} h}, \tag{11}$$

where h is the convection coefficient and $r_{\rm pi}$ the inner radius of the pipe.

The other thermal resistances inside the BHE can be determined by comparing our thermal circuit with that illustrated in Fig. 5. The thermal resistance between p_1 and p_2 can be obtained by subtracting $2R_{\rm conv}$ from R_{12}^{Δ}. The thermal resistance between p_1 and b can be obtained by subtracting $R_{\rm conv}$ from R_1^{Δ}. We chose to split this resistance in half by introducing the node gt_1, and we did the same for the resistance between p_2 and b, by introducing the node gt_2.

As for the ground, let r_0 be the radius of the BHE and r_i the outer radius of the i-th annulus. The thermal resistances $R_1, \dots R_{n+1}$ appearing in Fig. 2 are given by the equation:

$$R_i = \frac{1}{2\pi k_g} \ln\left(\frac{\bar{r}_i}{\bar{r}_{i-1}}\right), \tag{12}$$

where k_g is the thermal conductivity of the ground and

$$\bar{r}_i = \begin{cases} r_0 & \text{for } i = 0 \\ \sqrt{({r_{i-1}}^2 + r_i^2)/2} & \text{for } i = 1, \dots n \\ r_n & \text{for } i = n+1 \end{cases} \tag{13}$$

The partition of the ground, in the simple case of two concentric annuli, is illustrated in Fig. 7.

Note that $R_{\rm conv}$ and R_i, as well as R_1^{Δ}, R_{12}^{Δ}, $R_{\rm a}$ and $R_{\rm b}$, are thermal resistances per unit length. The corresponding thermal resistances in $\mathrm{K\,W^{-1}}$, for each horizontal layer of heigh l, are equal to the former divided by l.

Since each node models a portion of space filled with a given material, its heat capacity can be obtained multiplying the volume of the portion of space by the volumetric heat capacity ρc of the material. Thus, each ground node g_i has heat capacity

$$C_i = (\rho c)_g \pi ({r_i}^2 - {r_{i-1}}^2) l, \tag{14}$$

each fluid node has heat capacity

$$C_{\rm f} = (\rho c)_{\rm f} \pi r_{\rm pi}^2 l, \tag{15}$$

and each pipe node has heat capacity

$$C_{\rm p} = (\rho c)_{\rm p} \pi ({r_{\rm pe}}^2 - {r_{\rm pi}}^2) l, \tag{16}$$

where $r_{\rm pe}$ is the outer radius of the pipe. As for the grout, a single layer of height l has heat capacity

$$C_{\rm gt} = (\rho c)_{\rm gt} \pi ({r_0}^2 - 2\,{r_{\rm pe}}^2) l. \tag{17}$$

This is distributed among the nodes gt_1, gt_2 and b. We can then call $(1-\varepsilon)C_{\rm gt}$ the heat capacity of node b, and $(\varepsilon/2)C_{\rm gt}$ the heat capacity of each of the nodes gt_1 and gt_2, where ε is a number between 0 and 1.

Next, let us denote by a subscript j the lower surface of the j-th layer. Let us call $T_{{\rm f}1,j}$ and $T_{{\rm f}2,j}$ the temperatures of the fluid nodes, $T_{{\rm p}1,j}$ and $T_{{\rm p}2,j}$ the temperatures of the pipe nodes, $T_{{\rm gt}1,j}$ and $T_{{\rm gt}2,j}$ the temperatures of the grout nodes, $T_{0,j}$ the temperature of the borehole node, and $T_{1,j}, \dots, T_{n,j}$ the temperatures of the ground nodes, all measured at the lower surface of the of the j-th layer.

Since the two pipes of the BHE are connected at the bottom,

$$T_{{\rm f}1,m} = T_{{\rm f}2,m}. \tag{18}$$

Let us also call $T_{{\rm f}1,0} = T_{\rm in}$ the inlet fluid temperature and $T_{{\rm f}2,0} = T_{\rm out}$ the outlet fluid temperature. The energy balance equation yields

$$T_{{\rm f}1,0} = T_{{\rm f}2,0} + \frac{\dot{Q}}{\dot{m}_{\rm f} c_{\rm f}}, \tag{19}$$

where $\dot{m}_{\rm f}$ is the mass flow rate of the fluid and $\dot{Q}$ is the heat rate supplied to the BHE.

Finally, let us set the undisturbed ground temperature equal to zero. Namely,

$$T_{n+1\,j} = T_{\rm g} = 0. \tag{20}$$

Now, let us consider a set of time instants t_k, with $k = 0, 1, \dots, K$, where $t_0 = 0$ is the start of the heating. Assume that the temperatures of the nodes are constant for $t_k < t < t_{k+1}$, and that heat conduction in the vertical direction is negligible, so that energy transfer in the vertical direction takes place only through the fluid flow.

For every time instant (namely, for $k = 1, \dots, K$) and for every layer of height l (namely, for $j = 1, \dots, m$), the following balance equations hold.

1. Energy balance for the fluid nodes:

$$\dot{m}_{\rm f} c_{\rm f} \big(T_{{\rm f}1,j-1}(t_k) - T_{{\rm f}1,j}(t_k)\big) - \frac{T_{{\rm f}1,j}(t_k) - T_{{\rm p}1,j}(t_k)}{R_{\rm conv}/l} = C_{\rm f} \frac{T_{{\rm f}1,j}(t_k) - T_{{\rm f}1,j}(t_{k-1})}{t_k - t_{k-1}}, \tag{21}$$

$$\dot{m}_{\rm f} c_{\rm f} \big(T_{{\rm f}2,j}(t_k) - T_{{\rm f}2,j-1}(t_k)\big) - \frac{T_{{\rm f}2,j}(t_k) - T_{{\rm p}2,j}(t_k)}{R_{\rm conv}/l} = C_{\rm f} \frac{T_{{\rm f}2,j}(t_k) - T_{{\rm f}2,j}(t_{k-1})}{t_k - t_{k-1}}. \tag{22}$$

The first term of Eq. (21) represents the energy input per unit time to the fluid node $f_{1\,j}$, due to the difference between the temperature of the fluid entering the node and that of the fluid exiting the node. The second term represents the energy output per unit time from the fluid node $f_{1\,j}$ due to the heat transfer to the pipe node $p_{1\,j}$. The term at the right-hand side represents the energy stored per unit time in the fluid node $f_{1\,j}$. Eq. (22) is a similar energy balance, for the fluid node $f_{2\,j}$.

2. Energy balance for the pipe nodes:

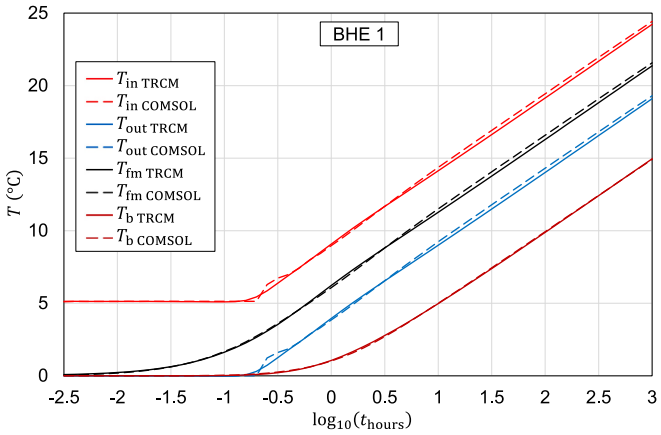

Fig. 8. Time evolutions of T_{in}, T_{out}, T_{fm} and T_b obtained by the TRCM and by the finite-element model, for BHE 1.

$$\frac{T_{f1,j}(t_k)-T_{p1,j}(t_k)}{R_{conv}/l}+\frac{T_{p2,j}(t_k)-T_{p1,j}(t_k)}{(R_{12}^{\Delta}-2R_{conv})/l}+\frac{T_{gt1,j}(t_k)-T_{p1,j}(t_k)}{\frac{1}{2}(R_1^{\Delta}-R_{conv})/l}=C_p\frac{T_{p1,j}(t_k)-T_{p1,j}(t_{k-1})}{t_k-t_{k-1}}, \tag{23}$$

$$\frac{T_{f2,j}(t_k)-T_{p2,j}(t_k)}{R_{conv}/l}+\frac{T_{p1,j}(t_k)-T_{p2,j}(t_k)}{(R_{12}^{\Delta}-2R_{conv})/l}+\frac{T_{gt2,j}(t_k)-T_{p2,j}(t_k)}{\frac{1}{2}(R_1^{\Delta}-R_{conv})/l}=C_p\frac{T_{p2,j}(t_k)-T_{p2,j}(t_{k-1})}{t_k-t_{k-1}}. \tag{24}$$

The first term of Eq. (23) represents the energy input per unit time to the pipe node $p_{1,j}$ due to the heat transfer from the fluid node $f_{1,j}$. The second term represents the energy input per unit time due to heat transfer from the pipe node $p_{2,j}$, and the third term represents the energy input per unit time due to the heat transfer from the grout node $gt_{1,j}$. The term at the right-hand side represents the energy stored per unit time in the pipe node $p_{1,j}$. Eq. (24) is a similar energy balance, for the pipe node $p_{2,j}$.

3. Energy balance for the grout nodes:

$$\frac{T_{p1,j}(t_k)-T_{gt1,j}(t_k)}{\frac{1}{2}(R_1^{\Delta}-R_{conv})/l}+\frac{T_{0,j}(t_k)-T_{gt1,j}(t_k)}{\frac{1}{2}(R_1^{\Delta}-R_{conv})/l}=\frac{\varepsilon}{2}C_{gt}\frac{T_{gt1,j}(t_k)-T_{gt1,j}(t_{k-1})}{t_k-t_{k-1}}. \tag{25}$$

$$\frac{T_{p2,j}(t_k)-T_{gt2,j}(t_k)}{\frac{1}{2}(R_1^{\Delta}-R_{conv})/l}+\frac{T_{0,j}(t_k)-T_{gt2,j}(t_k)}{\frac{1}{2}(R_1^{\Delta}-R_{conv})/l}=\frac{\varepsilon}{2}C_{gt}\frac{T_{gt2,j}(t_k)-T_{gt2,j}(t_{k-1})}{t_k-t_{k-1}}. \tag{26}$$

The first term of Eq. (25) represents the energy input per unit time to the grout node $gt_{1,j}$ due to the heat transfer from the pipe node $p_{1,j}$. The second term represents the energy input per unit time due to the heat transfer from the borehole node b_j. The term at the right-hand side represents the energy stored per unit time in the grout node $gt_{1,j}$. Eq. (26) is a similar energy balance, for the grout node $gt_{2,j}$.

4. Energy balance for the borehole node:

$$\frac{T_{1,j}(t_k)-T_{0,j}(t_k)}{R_1/l}+\frac{T_{gt1,j}(t_k)-T_{0,j}(t_k)}{\frac{1}{2}(R_1^{\Delta}-R_{conv})/l}+\frac{T_{gt2,j}(t_k)-T_{0,j}(t_k)}{\frac{1}{2}(R_1^{\Delta}-R_{conv})/l}=(1-\varepsilon)C_{gt}\frac{T_{0,j}(t_k)-T_{0,j}(t_{k-1})}{t_k-t_{k-1}}. \tag{27}$$

The first term of Eq. (27) represents the energy input per unit time to the borehole node b_j due to the heat transfer from the ground node $g_{1,j}$. The second term represents the energy input per unit time due to the heat transfer from the grout node $gt_{1,j}$, and the third term represents the energy input per unit time due to the heat transfer from the grout node $gt_{2,j}$. The term at the right-hand side represents the energy stored per unit time in the borehole node b_j.

5. Energy balance for the ground nodes:

$$\frac{T_{i-1,j}(t_k)-T_{i,j}(t_k)}{R_i/l}+\frac{T_{i+1,j}(t_k)-T_{i,j}(t_k)}{R_{i+1}/l}=C_i\frac{T_{i,j}(t_k)-T_{i,j}(t_{k-1})}{t_k-t_{k-1}}, \tag{28}$$

with $i=1,\ldots,n$.

The first term of Eq. (28) represents the energy input per unit time to the ground node $g_{i,j}$ due to the heat transfer from the ground node $g_{i-1,j}$. The second term represents the energy input per unit time due to the heat transfer from the ground node $g_{i+1,j}$. The term at the right-hand side represents the energy stored per unit time in the ground node $g_{i,j}$.

Eqs. (21–28), together with Eqs. (18) and (19), form a linear system of $(n+7)j+2$ equations in the unknowns $T_{f1,0}$, $T_{f2,0}$, $T_{f1,j}$, $T_{f2,j}$, $T_{p1,j}$, $T_{p2,j}$, $T_{gt1,j}$, $T_{gt2,j}$, $T_{0,j}$, $T_{1,j}$, …, T_{nj}. The system can be solved for increasing values of k. For $k=0$, all the temperatures are zero, except the inlet fluid temperature, $T_{f1,0}(0)$, which is given by Eq. (19).

4. Comparison between the results of the TRCM and those of the finite-element model

As explained in Section 2, the comparison between the results of the finite-element simulations with and without the high-conductivity layer suggests that it is not possible to reproduce exactly the time evolutions of R_{b3D} and of T_{fm} by means of a TRCM that employs the HUST assumption.

On the other hand, the comparison suggests that it is possible to get accurate values of T_b. For this purpose, we coded a C++ program that implements the TRCM illustrated in Section 3, for time-constant heat rate, with a selectable number of horizontal slices and a customizable partition of the ground. To obtain good accuracy, we performed our simulations with 100 horizontal slices and a finely partitioned ground: we set the thickness of the first ground annulus to 1 cm, the thickness increase ratio to 1.25, and the outer radius of the last ground annulus to be greater than 15 m, obtaining a total of 27 annuli. The simulations covered the time range from $10^{-2.5}$ hours to 10^3 hours, with steps of 0.1 in the logarithm of time in hours, after checking that a shorter time step did not change the results. As for the value of ε, after performing many simulations we decided to fix it to 0.3. This value of ε gave the lowest discrepancies between the simulation results obtained with the C++ program and those obtained with COMSOL.

The C++ program allows the user to change the geometrical and thermal parameters of the BHE, the number of horizontal layers and the partition of the ground. As output, the program yields the time evolutions of T_{in}, T_{out}, T_{fm}, T_b, R_{beff} and R_{b3D}.

The time evolutions of T_{in}, T_{out}, T_{fm}, and T_b obtained for BHE 1 using the C++ program are compared with those obtained by the finite-element model in Fig. 8. The figure shows that the TRCM determines rather accurately the time evolution of T_{in}, T_{out}, and T_{fm} up to $\log_{10}(t_{hours})\approx 0.6$, i.e. $t\approx 4$ hours, but slightly underestimates these temperatures for greater values of time. On the other hand, the TRCM determines the time evolution of T_b very accurately, with a RMSD of 0.037 °C with respect to the finite-element simulation.

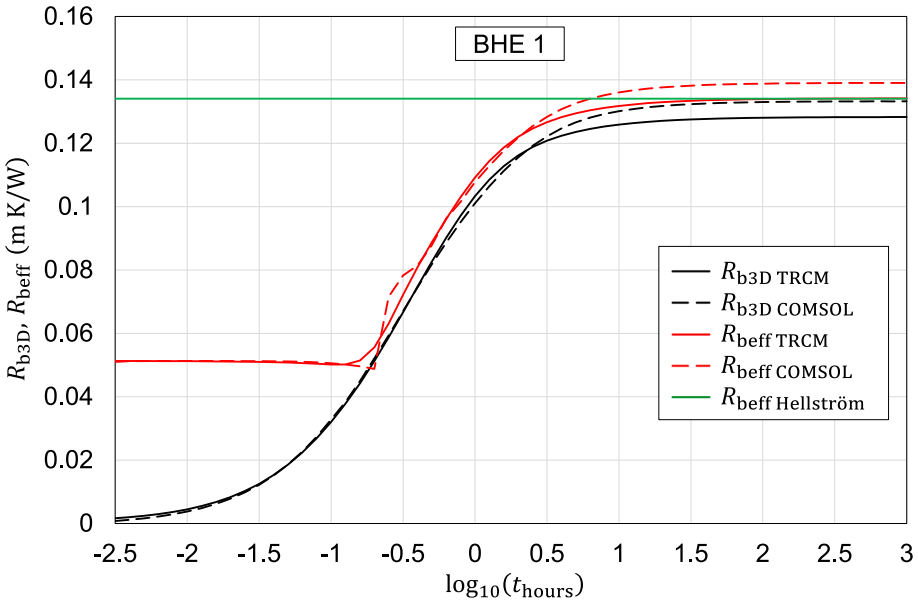

Fig. 9. Time evolutions of R_{b3D} and R_{beff} obtained by the TRCM and by the finite-element model, for BHE 1. The green line is the effective borehole thermal resistance given by Hellström's equation. (For interpretation of the references to colour in this figure legend, the reader is referred to the web version of this article.)

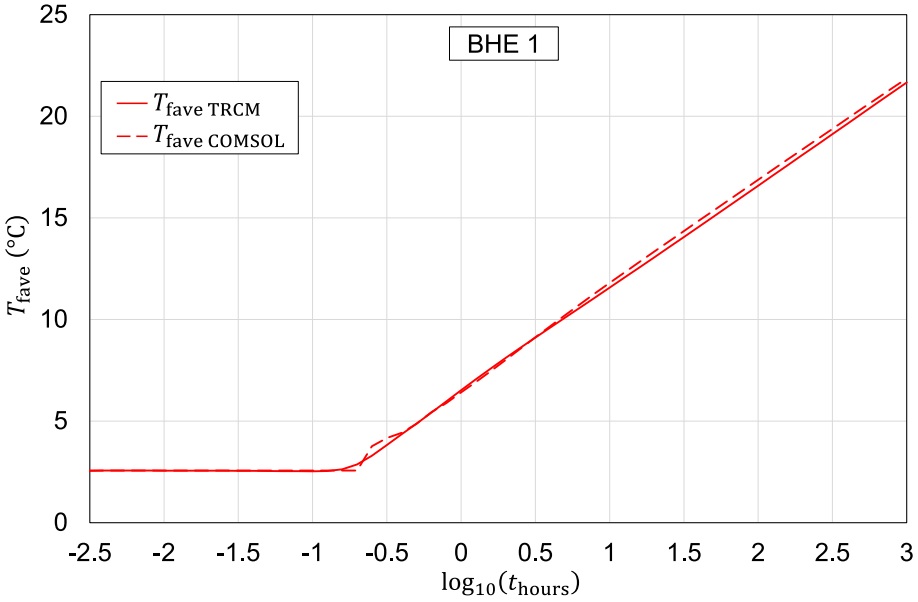

Fig. 10. Time evolution of T_{fave} obtained by the TRCM compared to that obtained by the finite-element model, for BHE 1.

As for R_{b3D} and R_{beff}, the results obtained for BHE 1 using the C++ program are compared with those obtained by the finite-element model in Fig. 9. The figure shows that the TRCM underestimates R_{b3D} and R_{beff} for $\log_{10}(t_{hours}) > 0.5$, and gives an asymptotic value of R_{beff} equal to the stationary value given by Hellström's equation, which is obtained under the assumption of isothermal surface of the BHE.

Another relevant quantity is the difference $T_{fave} - T_{fm}$, which allows you to calculate T_{fave} from T_{fm}, and vice versa. The time evolution of T_{fave} obtained using the C++ program is compared with that obtained by the finite-element model in Fig. 10. The figure shows that the TRCM slightly underestimates T_{fave} for $\log_{10}(t_{hours}) > 0.6$, and that the underestimation is quite similar to that of T_{fm} shown in Fig. 8. Therefore, one expects that the TRCM predicts accurately the time evolution of the difference $T_{fave} - T_{fm}$.

The time evolution of $T_{fave} - T_{fm}$ obtained for BHE 1 using the C++ program is compared with that obtained by the finite-element model in Fig. 11. The figure shows that the TRCM reproduces the time evolution of $T_{fave} - T_{fm}$ accurately, except in the range $-0.8 \leq \log_{10}(t_{hours}) \leq 0.5$, where the time evolution determined by COMSOL has an irregular trend. Analogous results to those obtained for BHE 1 have been found for all the BHEs studied in this paper.

In summary, the proposed TRCM determines correctly the time evolutions of T_b and of $T_{fave} - T_{fm}$, but slightly underestimates the time evolutions of T_{in}, T_{out}, T_{fm}, R_{b3D} and R_{beff} in the medium term. The underestimation is similar to the one observed for the finite-element simulation with the forced HUST condition. This reinforces the hypothesis that employing the HUST assumption causes unavoidable inaccuracies in the results of TRCMs.

To confirm this hypothesis, we compared the results of our simulations with those of the ANN developed by Pasquier and Marcotte [45].

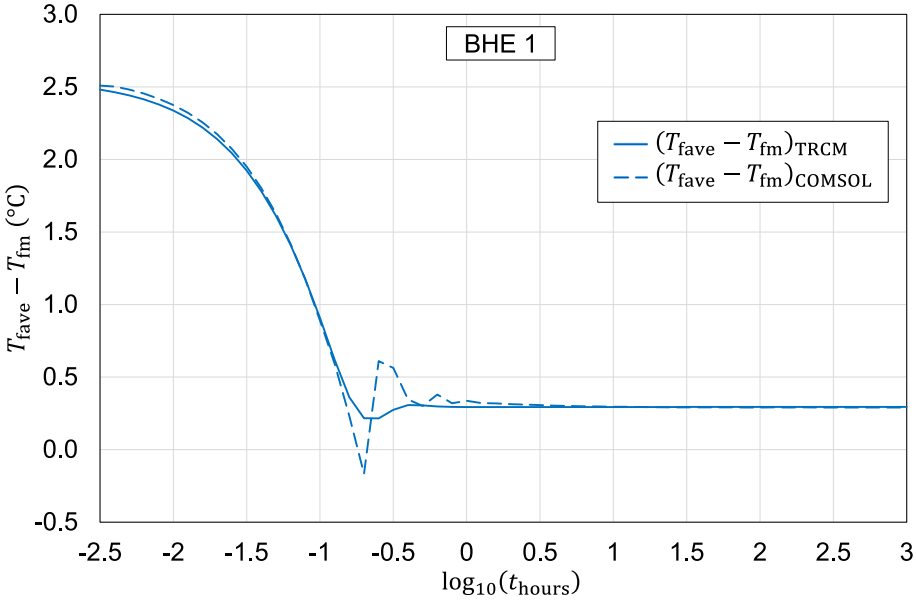

Fig. 11. Time evolution of $T_{fave} - T_{fm}$ obtained by the TRCM and by the finite-element model, for BHE 1.

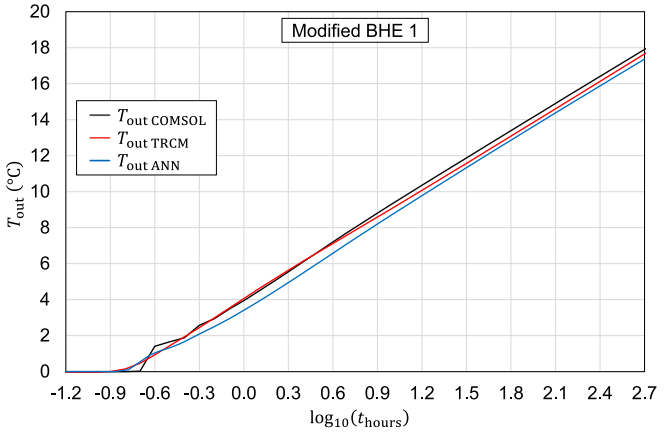

Fig. 12. Time evolution of T_{out} determined by COMSOL Multiphysics, by our TRCM, and by the ANN developed by Pasquier and Marcotte [44]. The results refer to a modified BHE 1, with $(\rho c)_p = 1.9 \mathrm{MJ}/(\mathrm{m}^3\mathrm{K})$, $\dot{V} = 16$ liters per minute and $R_{conv} = 10^{-6}$ m K/W.

The latter is based on the TRCM by Pasquier and Marcotte [37], which employs the HUST assumption. The MATLAB code of the ANN was kindly supplied by Pasquier.

For the comparison, a few changes were made to BHE 1. The volumetric heat capacity of the pipe was set to $1.9\ \mathrm{MJ}/(\mathrm{m}^3\mathrm{K})$ and the volume flow rate of the fluid to 16 liters per minute, since our original values were out of the range allowed by the ANN. Moreover, the convective thermal resistance per unit length between fluid and pipes was set to 10^{-6} m K/W, as in the ANN. The mean heat rate per unit length $\dot{q}_l = 50$ W/m was imposed in the ANN by setting $T_{in} - T_{out} = \frac{\dot{q}_l L}{\dot{V}(\rho c)_f} = 4.4893$ °C. The remaining input parameters are those listed in Table 1, fourth column.

The simulation of BHE 1, with the changes listed above, was performed with the ANN [45], with our TRCM and with COMSOL Multiphysics. A comparison of the time evolutions of T_{out} is illustrated in Fig. 12.

As expected, both our TRCM and the ANN [45] underestimate T_{out} for $\log_{10}(t_{hours}) > 0.6$, and the underestimation by the ANN is slightly larger.

The results of this section confirm that the HUST assumption causes an inevitable underestimation of the medium-term thermal response in TRCMs. This assumption, however, is necessary to use the correct expressions of the thermal resistances R_b and R_a. Therefore, the only way to obtain accurate time evolutions of T_{in}, T_{out}, T_{fm}, R_{b3D}, and R_{beff} by a TRCM, even in the medium term, is to introduce a correction factor a posteriori.

5. Improvement of the TRCM model by a correction factor

Since our TRCM predicts accurately the time evolution of T_b, we can deduce from Eq. (1) that the underestimation of T_{fm} is only due to that of R_{b3D}. Moreover, since our TRCM predicts accurately the time evolution of $T_{fave} - T_{fm}$, we can conclude that the underestimation of T_{fave} is almost the same as that of T_{fm}. Therefore, by correcting the time evolution of R_{b3D}, it is possible to get accurate values of both T_{fm} and T_{fave}. Finally, the corrected values of T_{fave} and the energy balance equation can be used to obtain accurate values of T_{in} and T_{out}, while the corrected values of R_{beff} can be obtained from Eq. (2).

In short, the inaccuracies of the TRCM can be nearly completely resolved by determining, for each U-tube BHE, a time-dependent correction coefficient that transforms the time evolution of R_{b3D} given by the TRCM into that given by the finite-element simulation.

We define the correction coefficient as

$$c_{coeff} = \frac{R_{b3D,COMSOL}}{R_{b3D,TRCM}}. \tag{29}$$

This way, the product $c_{coeff}\, R_{b3D,TRCM}$ yields a corrected value of the 3D borehole thermal resistance, which we will call $R_{b3D,c}$, equal to the one determined by COMSOL.

Once the correction coefficient is known, the corrected values of the mean, the average, the inlet and the outlet fluid temperature, $T_{fm,c}$, $T_{fave,c}$, $T_{in,c}$, $T_{out,c}$, and the corrected values of the effective borehole thermal resistance, $R_{beff,c}$, can then be determined as follows:

$$T_{fm,c} = T_b + \dot{q}_l R_{b3D,c}, \tag{30}$$

$$T_{fave,c} = T_{fm,c} + \left(T_{fave} - T_{fm}\right), \tag{31}$$

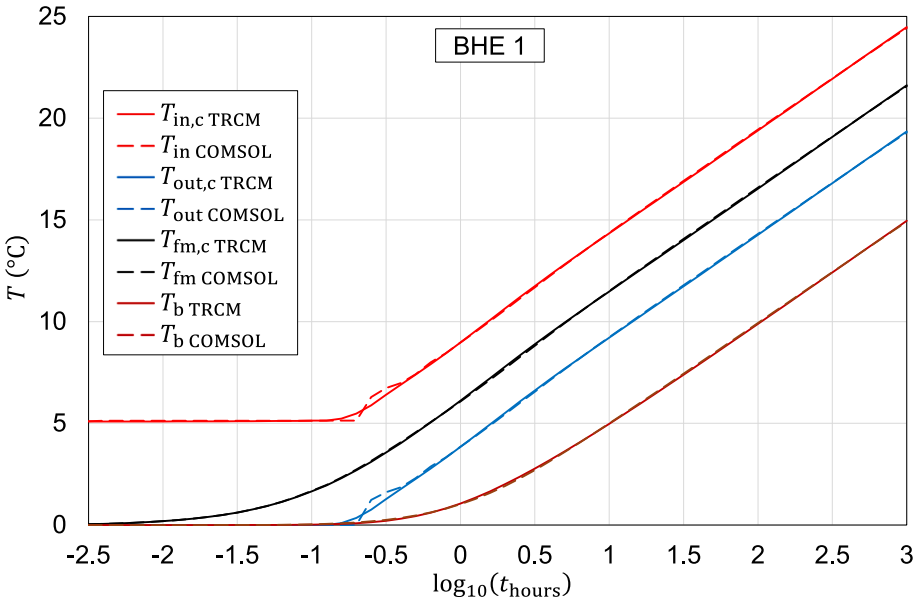

Fig. 13. Time evolutions of T_{in}, T_{out}, T_{fm} and T_b obtained by the corrected TRCM and by the finite-element simulation run with COMSOL Multiphysics, for BHE 1.

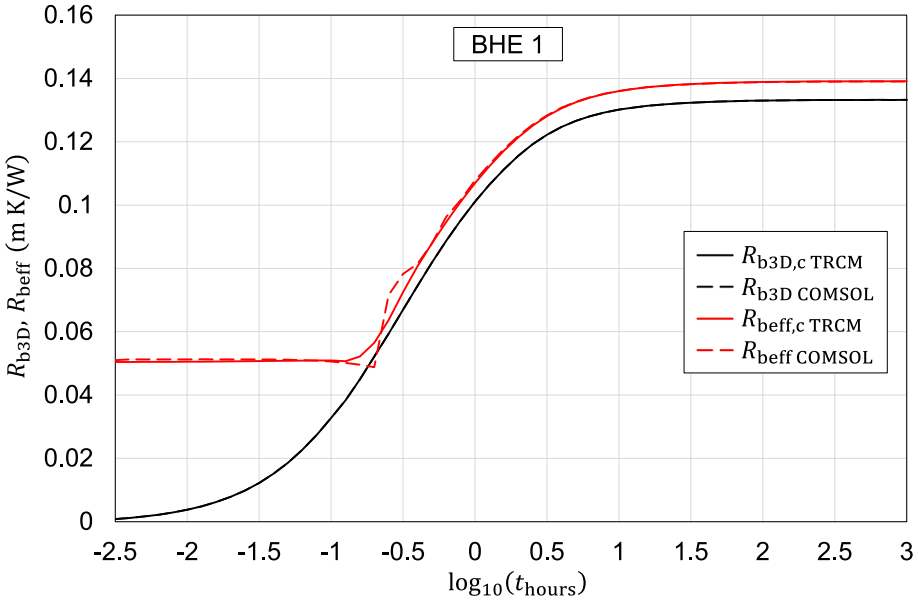

Fig. 14. Time evolutions of R_{b3D} and R_{beff} obtained by the corrected TRCM and by the finite-element simulation run with COMSOL Multiphysics, for BHE 1.

$$T_{in,c} = T_{fave,c} + 0.5\frac{\dot{Q}}{\dot{m}c_f}, \tag{32}$$

$$T_{out,c} = T_{fave,c} - 0.5\frac{\dot{Q}}{\dot{m}c_f}. \tag{33}$$

$$R_{beff,c} = \frac{1}{\dot{q}_l}\left(T_{fave,c} - T_b\right). \tag{34}$$

Since T_b is already estimated accurately, there is no need to correct it.

In this paper, we determined the time evolution of c_{coeff} for shallow U-tube BHEs, with lengths ranging from 60 to 200 m, subjected to a time-constant heat rate. The values of c_{coeff} hold also for BHEs with length between 40 and 60 m, up to the dimensionless time $t^* = 0.002$. These ranges of BHE length cover nearly all the BHE fields installed and planned for installation in Italy, where medium depth BHEs appear less attractive due to the combined need for heating and cooling. Our TRCM applies to any U-tube BHE long enough to make the axial conduction in the solid negligible, but the application to medium depth BHEs would only be meaningful if a geothermal gradient were introduced. Upgrading the model to this condition would not be difficult, but calculating c_{coeff} for cases with appreciable effects of the geothermal gradient would require an analysis that has not yet been done.

Several pairs of simulations, performed by COMSOL Multiphysics and by the TRCM, showed that only four parameters have a relevant effect on the correction coefficient: the borehole radius, r_b, the shank spacing, s, the thermal conductivity of the grout, k_{gt}, and the outer radius of the pipe, r_{pe}. This conclusion was reached after analyzing the effects on c_{coeff} of other potentially relevant parameters, such as the BHE length, the flow rate, the volumetric heat capacities of the grout and the ground, the thermal conductivity of the ground. Although these parameters influence R_{b3D}, we found that they have a negligible effect on the ratio of $R_{b3D,COMSOL}$ to $R_{b3D,TRCM}$.

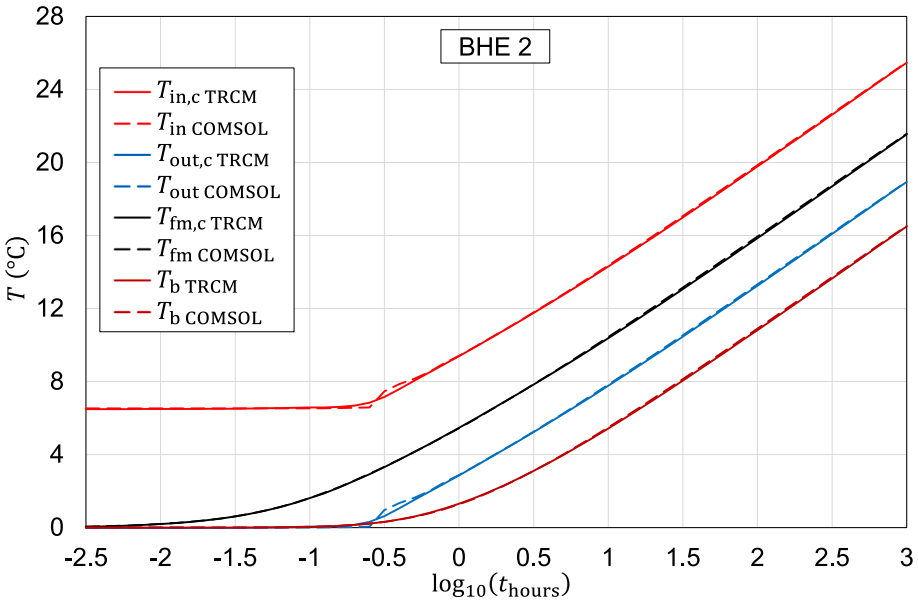

Fig. 15. Time evolutions of T_{in}, T_{out}, T_{fm} and T_b obtained by the corrected TRCM and by the finite-element simulation run with COMSOL Multiphysics, for BHE 2.

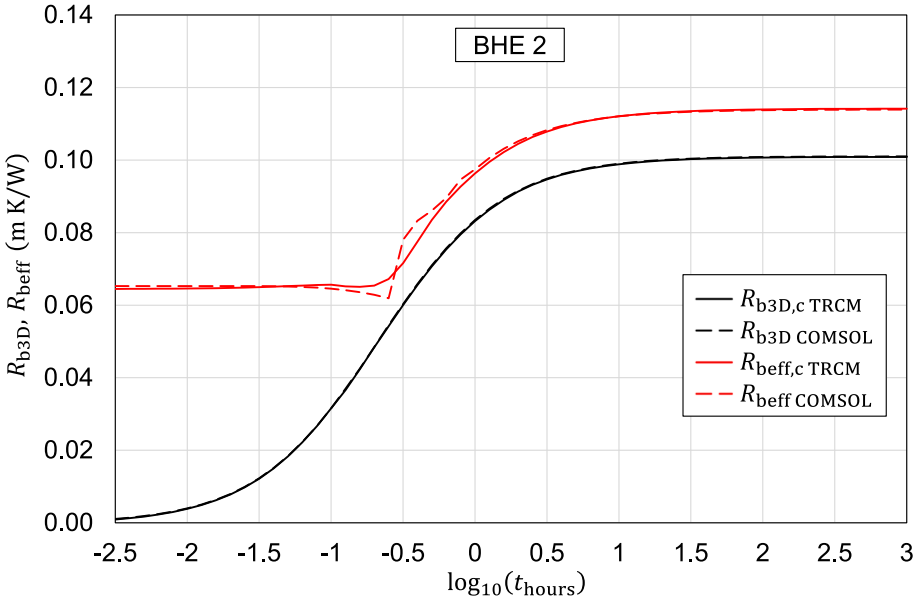

Fig. 16. Time evolutions of R_{b3D} and R_{beff} obtained by the corrected TRCM and by the finite-element simulation run with COMSOL Multiphysics, for BHE 2.

Since single U-tube BHEs usually have standard pipes, with $r_{pe} = 20$ mm or $r_{pe} = 16$ mm, we selected these two values. For each value of r_{pe}, we considered three values of r_b, namely 68, 72 and 76 mm, three values of s, namely 27, 37 and 47 mm, and three values of k_{gt}, namely 1.0, 1.6 and 2.2 W/(m K). For the BHEs with $r_{pe} = 20$ mm, we set $r_{pi} = 16.3$ mm and $\dot{V}_f = 14$ liters per minute; for the BHEs with $r_{pe} = 16$ mm, we set $r_{pi} = 13$ mm and $\dot{V}_f = 12$ liters per minute. The selected values of r_{pi} are those corresponding to r_{pe} in the standard pipes. We kept fixed all the remaining parameters, with the following values: $L = 100$ m, $(\rho c)_{gt} = 2.5$ MJ/(m^{3}K), $k_g = 1.8$W/(m K), $(\rho c)_g = 2.8$ MJ/(m^{3}K), and D, k_p, $(\rho c)_p$, $\dot{q}_l$ with the values reported in Table 1. We selected water as the working fluid, with properties evaluated at 20 °C. In total, we ran 54 pairs of simulations with COMSOL Multiphysics and with the TRCM, 27 for each value of r_{pe}, obtaining 54 time-dependent values of c_{coeff}, in the time range from $10^{-2.5}$ hours to 10^3 hours. The simulations with COMSOL Multiphysics were performed as described in Section 2, and the simulations with the TRCM were performed as described in Section 4. The R_{b3D} values determined by COMSOL and the correction coefficients have been collected in an Excel file, available at the data repository of the University of Bologna.

A run option has been implemented in the C++ program, where the 54 time-dependent values of c_{coeff} are used to correct the values of T_{in}, T_{out}, T_{fm}, R_{beff}, and R_{b3D}. If this option is chosen, parabolic interpolations are performed to estimate the correction factor for the values of r_b, s, and k_{gt} set in the input file. A linear interpolation in r_{pe} is also performed in case its value is neither 20 nor 16 mm.

6. Results

The time evolutions of T_{in}, T_{out}, T_{fm}, T_b, R_{b3D} and R_{beff} obtained by the corrected TRCM have been compared with those determined by the

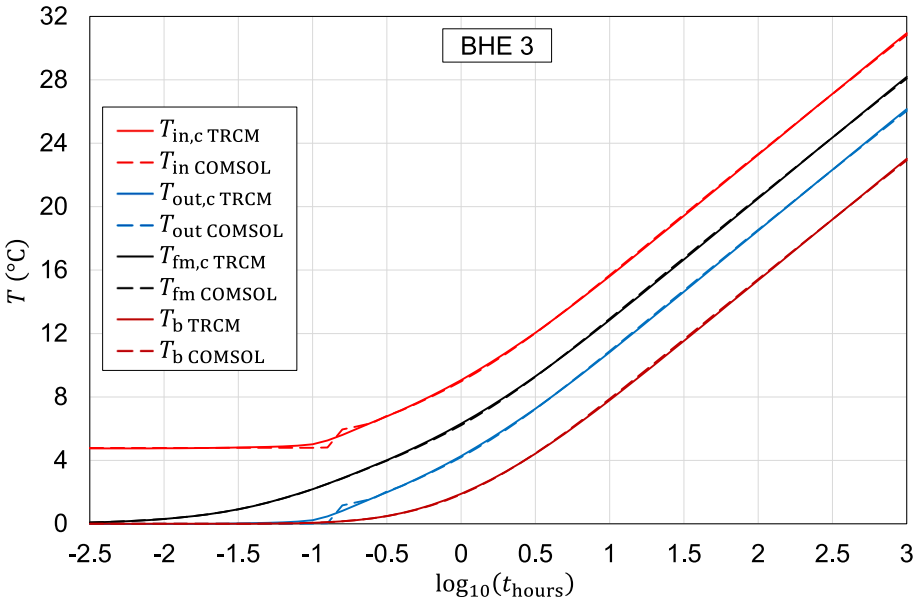

Fig. 17. Time evolutions of T_{in}, T_{out}, T_{fm} and T_b obtained by the corrected TRCM and by the finite-element simulation run with COMSOL Multiphysics, for BHE 3.

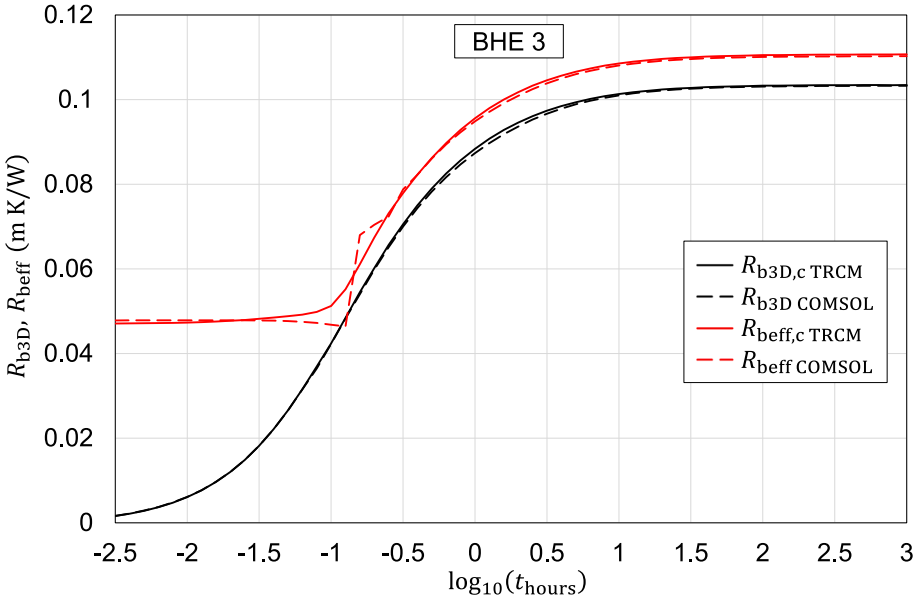

Fig. 18. Time evolutions of R_{b3D} and R_{beff} obtained by the corrected TRCM and by the finite-element simulation run with COMSOL Multiphysics, for BHE 3.

finite-element model for several single U-tube BHEs. An excellent agreement was found in all cases, except for small differences in the time evolutions of T_{in}, T_{out}, and R_{beff} in the time ranges where the values given by COMSOL Multiphysics have an irregular trend. As examples, three BHEs are considered in this section: BHE 1, BHE 2 and BHE 3, whose geometrical and thermal parameters are reported in Table 1.

In the case of BHE 1, a particularly good agreement is expected between the finite-element model and the corrected TRCM. Indeed, BHE 1 is one of the 54 BHEs used to evaluate the correction coefficients, so no interpolation is required to apply the correction factor.

The time evolutions of T_{in}, T_{out}, and T_{fm} obtained for BHE 1 by the corrected TRCM are compared with those determined by the finite-element model in Fig. 13. The figure reveals an excellent agreement between the two models. The RMSD between the values of T_{fm} given by the two simulations is 0.037 °C.

The RMSD between the values of T_b is also 0.037 °C, as reported in Section 4. As for T_{in} and T_{out}, the values given by the corrected TRCM in time range $-0.8 \le \log_{10}(t_{hours}) \le -0.4$ are smoothed compared to those determined by COMSOL. Excluding this time range, the agreement between the two pairs of curves is excellent, with a RMSD of 0.038 °C for T_{in} and 0.039 °C for T_{out}.

The time evolutions of R_{b3D} and R_{beff} for BHE 1 are illustrated in Fig. 14. Since BHE 1 is one the 54 BHEs used to evaluate the correction factors, the values of R_{b3D} given by the two simulations are identical. Similarly to what we observed for T_{in} and T_{out}, the values of R_{beff} given by the corrected TRCM in time range $-0.8 \le \log_{10}(t_{hours}) \le -0.4$ are smoothed compared to those determined by COMSOL. Excluding this time range, the RMSD between the R_{beff} values is 4.7×10^{-4}m K/W. At the final instant $t = 1000$ hours, the value of R_{beff} given by the corrected TRCM is 9.2×10^{-5}m K/W greater than the one determined by COMSOL (namely, 0.066% greater).

Unlike BHE 1, almost all the parameters of BHE 2 are different from

Table 2
TRT data reported in [37,48].

Quantity	Symbol	Unit	Value
Pipe thermal conductivity	k_p	W/(m K)	0.74
Grout thermal conductivity	k_{gt}	W/(m K)	1.90
Ground thermal conductivity	k_g	W/(m K)	3.02
Fluid volumetric heat capacity	$(\rho c)_f$	MJ/(m^{3}K)	4.20
Pipe volumetric heat capacity	$(\rho c)_p$	MJ/(m^{3}K)	1.8484
Grout volumetric heat capacity	$(\rho c)_{gt}$	MJ/(m^{3}K)	1.89
Ground volumetric heat capacity	$(\rho c)_g$	MJ/(m^{3}K)	2.25
Pipe outer radius	r_{pe}	m	0.021
Pipe inner radius	r_{pi}	m	0.017
Half shank spacing	s	m	0.050
BHE radius	r_b	m	0.076
BHE length	H_b	m	138.99
Volume flow rate	$\dot{V}$	liters/s	0.435
Undisturbed ground temperature	T_g	°C	7.49
Fluid convective resistance	R_{conv}	mK/W	0.006

those used to determine the correction coefficients. In this case, the correction factor applied to the TRCM is estimated by the interpolation techniques mentioned in Section 5.

The time evolutions of T_{in}, T_{out}, T_{fm} and T_b obtained for BHE 2 by the corrected TRCM are compared with those determined by the finite-element model in Fig. 15. The agreement between the two models is still excellent. The RMSD between the values of T_{fm} by the two simulations is 0.051 °C. The RMSD between the values of T_b is 0.047 °C. As for T_{in} and T_{out}, the values given by the corrected TRCM in time range $-0.8 \leq \log_{10}(t_{hours}) \leq -0.3$ are smoothed compared to those determined by COMSOL. Excluding this time range, the agreement between the two pairs of curves is excellent, with a RMSD of 0.048 °C for T_{in} and 0.049 °C for T_{out}.

The time evolutions of R_{b3D} and R_{beff} for BHE 2 are illustrated in Fig. 16. The RMSD between the R_{b3D} values of the two simulations is 1.82×10^{-4}m K/W. At $t = 1000$ hours, the value of R_{b3D} given by the corrected TRCM is 1.54×10^{-4}m K/W lower than the one determined by COMSOL (namely, 0.13% lower). The values of R_{beff} given by the corrected TRCM in time range $-1 \leq \log_{10}(t_{hours}) \leq 0$ are smoothed

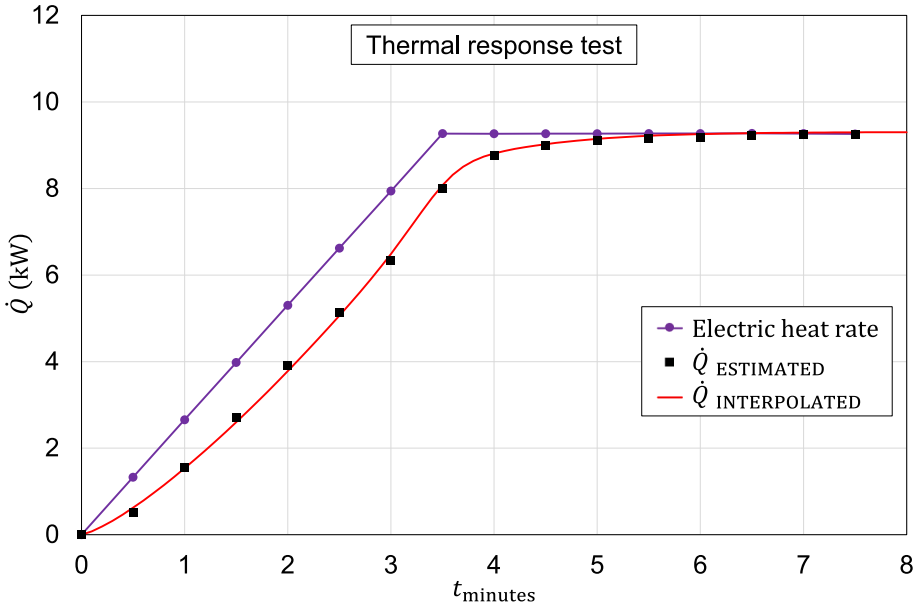

Fig. 19. Time evolutions of the electric heat rate, of the heat rate given by Eq. (35), and of the heat rate given by Eq. (36) during the first 7.5 min of the heating part of the TRT.

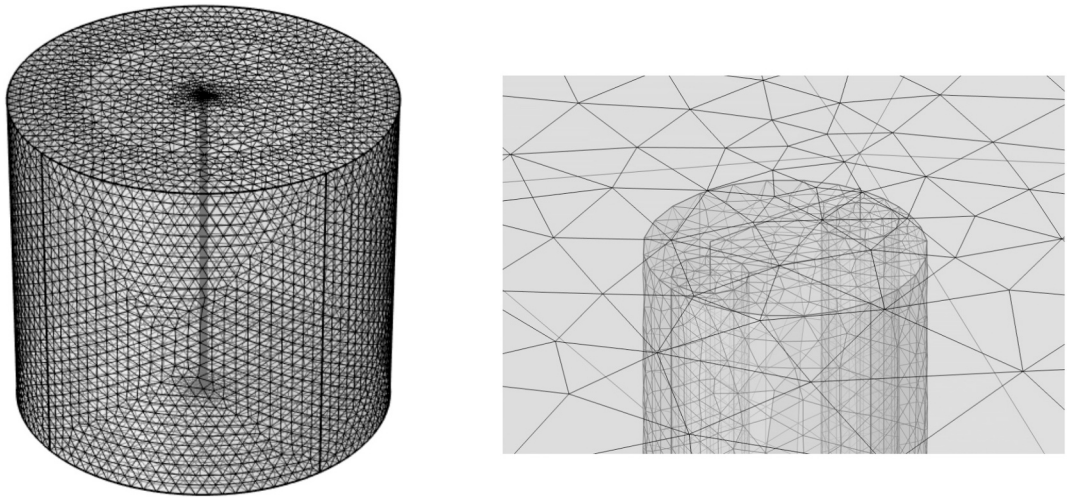

Fig. 20. Mesh employed in the simulation of the TRT described in [37]: complete meshed domain (left) and particular at the BHE top (right).

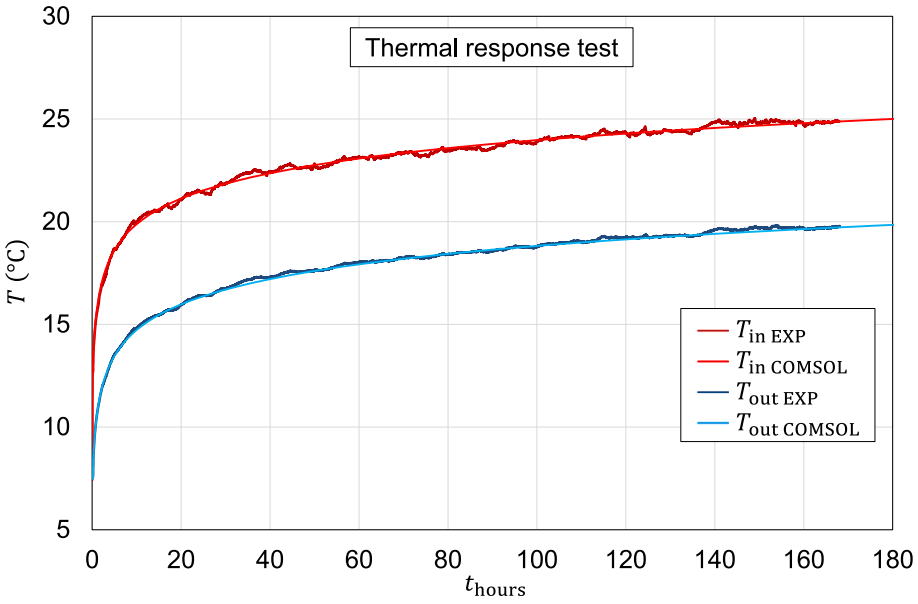

Fig. 21. Time evolutions of T_{in} and T_{out} obtained experimentally, compared with those obtained by the finite-element simulation, in the real time scale.

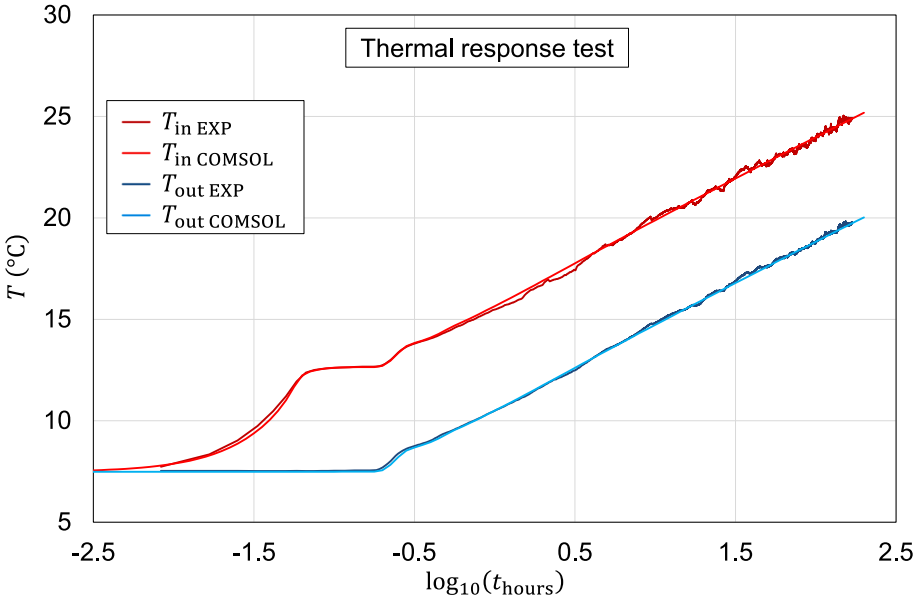

Fig. 22. Time evolutions of T_{in} and T_{out} obtained experimentally, compared with those obtained by the finite-element simulation, in the logarithmic time scale.

compared to those determined by COMSOL.

Excluding this time range, the RMSD between the R_{beff} values is 4.61×10^{-4} m K/W. At $t = 1000$ hours, the value of R_{beff} given by the corrected TRCM is 2.59×10^{-4}m K/W greater than the one determined by COMSOL (namely, 0.23% greater).

As for BHE 3, not only do its parameters differ from those used to determine the correction coefficients, but the borehole radius, $r_b = 64$ mm, is smaller than the lowest value employed in the parabolic interpolation. This value of r_b was chosen on purpose, to test the accuracy of the corrected TRCM in cases where extrapolation is required.

The time evolutions of T_{in}, T_{out}, T_{fm} and T_b obtained for BHE 3 by the corrected TRCM are compared with those determined by the finite-element model in Fig. 17. The agreement between the two models is, once again, remarkable. The RMSD between the values of T_{fm} given by the two simulations is 0.052 °C. The RMSD between the values of T_b is 0.049 °C. As for T_{in} and T_{out}, the values given by the corrected TRCM in time range $-1.2 \leq \log_{10}(t_{hours}) \leq -0.7$ are smoothed compared to those determined by COMSOL. Excluding this time range, the agreement between the two pairs of curves is excellent, with a RMSD of 0.052 °C both for T_{in} and T_{out}.

The time evolutions of R_{b3D} and R_{beff} for BHE 3 are illustrated in Fig. 18. The RMSD between the R_{b3D} values of the two simulations is 4.40×10^{-4} m K/W. At $t = 1000$ hours, the value of R_{b3D} given by the corrected TRCM is 2.10×10^{-4} m K/W greater than the one determined by COMSOL (namely, 0.20% greater). The values of R_{beff} given by the corrected TRCM in time range $-1.5 \leq \log_{10}(t_{hours}) \leq -0.5$ are smoothed compared to those determined by COMSOL. Excluding this time range, the RMSD between the R_{beff} values is 5.26×10^{-4} m K/W. At $t = 1000$ hours, the value of R_{beff} given by the corrected TRCM is 4.43×10^{-4} m K/W greater than the one determined by COMSOL (namely, 0.40% greater).

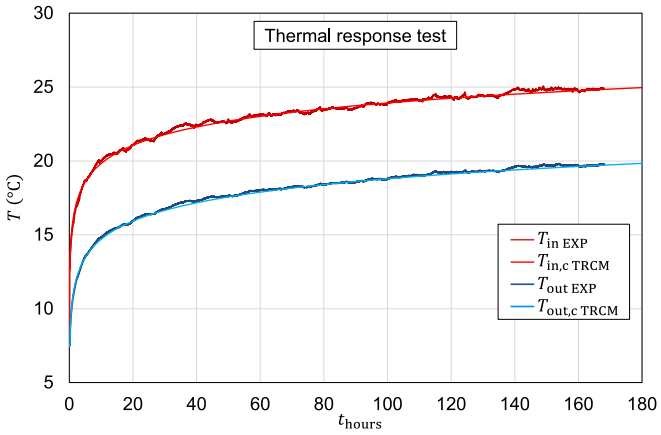

Fig. 23. Time evolutions of T_{in} and T_{out} obtained experimentally, compared with those obtained by our TRCM with correction, in the real time scale.

7. Validation by experimental data

Our COMSOL model was validated in [16] by comparison with a finite-element conduction model, where the fluid flow was replaced by a high-conductivity solid with heat generation, and with the FLS solution of Claesson and Javed [1]. The validation was performed by employing a modified geometry, with only one downpipe, so that the different models could yield the same results. Our TRCM was validated against the COMSOL model in Section 6.

Another validation of both the COMSOL model and the TRCM is presented here, by reproducing the time evolution of T_{in} and T_{out} in the heating part of a TRT performed by Pasquier and Groleau [48], and reconsidered in [37].

The ground was composed of 10.7 m of silty sand lying over a bedrock composed of sequences of red slate, and grey, greeny and red mud-slate. The water level was 0.72 m below the ground surface, and no appreciable groundwater flow was detected. The BHE was composed of loop of two thermally enhanced HDPE pipes, installed from the surface down to a depth of 138.99 m. Spacers were installed at every 1.5 m. The filling material was made of xenomorph to automorph quartz particles from the BHE base up to a depth of 16.76 m, and of bentonite slurry and sand up to the BHE top. The BHE data reported in [48] and in [37] are here recalled in Table 2.

Note that the pipe outer radius and the volume flow rate are larger than the highest values employed in the parabolic interpolation of c_{coeff}, and the thermal conductivity of the pipe is much higher than that considered in the parabolic interpolation.

The TRT data were collected every half minute, and the heating period lasted 168 h, with a total of 20,161 values for each quantity. The working fluid was water, and mean heat rate during heating was 9306.8 W, corresponding to 66.96 W/m.

The water volume in the above-ground piping was rather small, namely 15 to 18 l. Even in this case, the heating rate $\dot{Q}$ supplied to the inlet section of the BHE did not correspond to the electric heating rate, during the first minutes. We estimated the time evolution of $\dot{Q}$ during the first 7.5 min by the energy balance

$$\dot{Q}(t) = \dot{m}_f(t) c_f [T_{in}(t) - T_{in}(0)], \tag{35}$$

with the measured values of $\dot{m}_f(t)$ and $T_{in}(t)$. To facilitate data entry into our simulation codes, we interpolated the values given by Eq. (35) with the following function:

$$\dot{Q}(t) = 9306.8 \left[\frac{0.165(t/60)^{1.3}}{1 + e^{5(t/60-3.5)}} + \frac{1 - 0.105\, e^{-1.2(t/60-3.5)}}{1 + e^{-5(t/60-3.5)}} \right], \tag{36}$$

where t is time in seconds and $\dot{Q}(t)$ is in watt. The values of the electric heat rate, of $\dot{Q}(t)$ estimated by Eq. (35), and of $\dot{Q}(t)$ given by Eq. (36) are illustrated in Fig. 19. Since Eq. (36) rapidly converges to the mean heat rate of 9306.8 W, it was used for the whole simulation of the TRT.

The TRT simulation of by COMSOL Multiphysics was performed with the model used in the previous sections and with modified input data. The TRT data used are those reported in Table 2, with the exception of the fluid convective resistance. The latter was calculated by the software by considering water at 20 °C as the working fluid, with the properties reported in [46]. Due to the short operation time considered, the computational domain radius was reduced to 4 m and the computational domain height was set equal to the BHE length plus 3 m, divided by the scaling factor 20. The mesh employed in the final computations was the extra fine mesh built by the software, and consisted of 1,093,032 tetrahedral elements. It is illustrated in Fig. 20.

The results obtained with this mesh were considered as definitive, because they were very close to those obtained with a coarser mesh

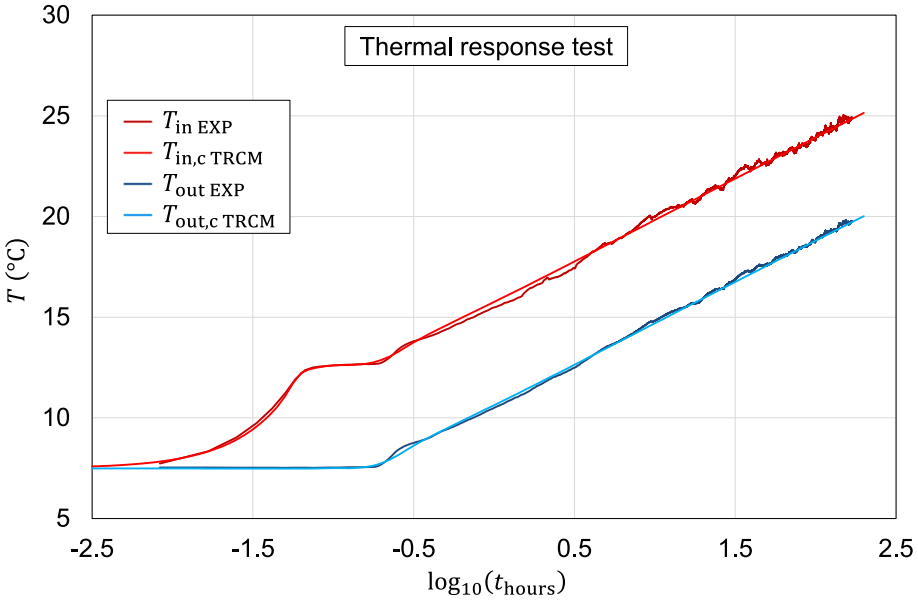

Fig. 24. Time evolutions of T_{in} and T_{out} obtained experimentally, compared with those obtained by our TRCM with correction, in the logarithmic time scale.

composed of 252,272 tetrahedral elements. The simulation results were collected in the time interval from 10^{-4} hours to $10^{2.3}$ hours, with steps of 0.05 in the logarithmic scale.

Many simulations were performed in order to obtain the values of k_g, k_{gt}, $(\rho c)_g$, and $(\rho c)_{gt}$ that better reproduce the experimental time evolutions T_{in} and T_{out}. For each set of values of the above-mentioned parameters, the RMSD between the experimental and the simulated values of T_{in} and T_{out} was determined by considering 86 instants of time in the logarithmic scale, from $10^{-2.05}$ hours to $10^{2.3}$ hours. The experimental values of T_{in} and T_{out} in these time instants were calculated by interpolations of the experimental data, performed through the function Interpolation of Mathematica. The optimal values of k_g, k_{gt}, $(\rho c)_g$, and $(\rho c)_{gt}$ thus determined are: $k_g = 3.02\ \mathrm{W/(m\,K)}$, $k_{gt} = 2.0\ \mathrm{W/(m\,K)}$, $(\rho c)_g = 2.4\ \mathrm{MJ/(m^3K)}$, $(\rho c)_{gt} = 2.7\ \mathrm{MJ/(m^3K)}$. The corresponding RMSDs are 0.143 °C for T_{in}, and 0.075 °C for T_{out}.

Our optimal parameter values are in overall good agreement with those reported in [37]. The values of k_g coincide, and the values of k_{gt} are almost coincident. The value of $(\rho c)_g$ we found is slightly higher than the one reported in [37], and the value of $(\rho c)_{gt}$ is significantly higher. Significant discrepancies between the values of $(\rho c)_{gt}$ obtained in TRT simulations are very common, because a precise estimate of this parameter is almost impossible.

A comparison between the experimental time evolutions of T_{in} and T_{out} and those obtained through the finite-element simulation with the optimal values of the parameters is illustrated in Fig. 21, in the real time scale, and in Fig. 22, in the logarithmic time scale. Fig. 22 shows, in particular, an excellent agreement between experimental and simulated values even in the first minutes of heating, a result non easily achieved.

To verify the accuracy of our TRCM in simulating TRTs, the simulation of the TRT considered in [37] was repeated with our TRCM, using the same COMSOL input data. The simulation was performed in the time interval from $10^{-2.5}$ hours to $10^{2.3}$ hours with steps of 0.05 in the logarithmic scale, with 100 horizontal slices, thickness of the first ground annulus 1 cm, thickness increase ratio 1.25, outer radius of the last ground annulus greater than 15 m.

A comparison between the experimental time evolutions of T_{in} and T_{out} and those obtained through the TRCM with correction is illustrated in Fig. 23, in the real time scale, and in Fig. 24, in the logarithmic time scale.

The figures show an excellent agreement between the experimental and the simulated values, even if some BHE parameters were out of the range considered in the interpolations. The RMSD between experimental and simulated values, considering 86 instants of time in the logarithmic scale from $10^{-2.05}$ hours to $10^{2.3}$ hours, is 0.170 °C for T_{in}, and 0.102 °C for T_{out}. The computation time with COMSOL Multiphysics was 4 h, while that with the TRCM was 2 s, which is 7200 times faster.

8. Conclusions

In Thermal Resistance Capacity Models (TRCMs) of borehole heat exchangers (BHEs), the borehole wall is usually considered as horizontally isothermal, and is represented by one node at each depth. This is necessary in order to use the accurate expressions of the thermal resistances between each pipe and the borehole wall, and between the pipes, calculated by the multipole method.

We have shown that this assumption yields slight inaccuracies in the prediction of the time evolution of the inlet and outlet fluid temperatures, T_{in} and T_{out}, of the mean fluid temperature, T_{fm}, of the 3D borehole thermal resistance, R_{b3D}, and of the effective borehole thermal resistance, R_{beff}, while it has no considerable effect on the time evolution of the mean surface temperature of the BHE, T_b.

This conclusion was reached by comparing two accurate finite-element simulations of a single U-tube BHE subjected to a constant heat rate, with and without a thin high-conductivity layer, adjacent to the BHE surface, that forces this surface to be horizontally isothermal. The simulations were implemented in COMSOL Multiphysics, and the energy balance along the flow was simulated through the Pipe Flow Module.

A TRCM of single U-tube BHEs has been developed. The model, which assumes a horizontally isothermal BHE surface, confirms the results obtained by the finite-element simulations: it slightly underestimates T_{in}, T_{out}, T_{fm}, R_{b3D} and R_{beff}, but yields accurate time evolutions of T_b. The model also yields an accurate time evolution of the difference $T_{fm} - T_{fave}$, where T_{fave} is the arithmetic mean of the inlet and outlet temperatures.

The accurate values of T_b and $T_{fm} - T_{fave}$ have been exploited to design a method that corrects the results of the TRCM a posteriori. To this purpose, 54 pairs of simulations were performed, with our TRCM and with COMSOL Multiphysics, for different types of single U-tube BHEs. The results of the simulations were used to determine a time-dependent correction coefficient, c_{coeff}, that transforms the time evolution of R_{b3D} calculated by our TRCM into that given by the COMSOL. The accurate time evolutions of T_b and $T_{fave} - T_{fm}$, together with the corrected values of R_{b3D}, were used to obtain, by simple mathematical relations, accurate time evolutions of T_{in}, T_{out}, T_{fm}, and R_{beff}.

The proposed TRCM and the correction method have been implemented in a C++ program, available at the open-source online data repository of the University of Bologna. The program yields, within two seconds, the same time evolutions of T_b, T_{in}, T_{out}, T_{fm}, R_{b3D}, and R_{eff} as those yielded by an accurate finite-element simulation requiring several hours of computation time. The results hold for any single U-tube BHE subjected to a time-constant heat rate, in a working period from $10^{-2.5}$ hours (about 11 s) up to 10^3 hours for BHE length greater than 60 m, or up to the dimensionless time $t^* = 0.002$ for BHE length between 40 and 60 m.

The TRCM and the correction method have been successfully validated against a TRT. The agreement between experimental and simulated values of the inlet and outlet fluid temperatures was excellent, and nearly identical to that obtained with COMSOL, with a computation time 7200 times shorter.

Possible applications of the program are the numerical evaluation of TRTs and the determination of accurate time dependent and asymptotic values of R_{b3D} and R_{beff}, to be employed in programs that provide the full-time-scale thermal response of a bore field subjected to a time-constant heat load.

CRediT authorship contribution statement

Enzo Zanchini: Writing – review & editing, Writing – original draft, Validation, Software, Methodology, Investigation, Formal analysis, Data curation, Conceptualization. **Francesco Zanchini:** Writing – review & editing, Writing – original draft, Visualization, Software, Methodology, Formal analysis, Data curation. **Claudia Naldi:** Writing – review & editing, Writing – original draft, Visualization, Software, Methodology, Data curation.

Declaration of competing interest

The authors declare that they have no known competing financial interests or personal relationships that could have appeared to influence the work reported in this paper.

Acknowledgements

The authors are grateful to Professor Philippe Pasquier for providing the MATLAB code of the ANN developed in Pasquier and Marcotte [45], and the data set of the TRT performed by Pasquier and Groleau [48].

Data availability

The C++ simulation program developed by the model is available at the AMS Acta UNIBO Repository, DOI 10.6092/unibo/amsacta/8580

References

[1] J. Claesson, S. Javed, An analytical method to calculate borehole fluid temperatures for time-scales from minutes to decades, ASHRAE Trans. 117 (2011) 279–288.

[2] M. Fossa, The temperature penalty approach to the design of borehole heat exchangers for heat pump applications, Energ. Buildings 43 (2011) 1473–1479, https://doi.org/10.1016/j.enbuild.2011.02.020.

[3] V. Malayappan, J.D. Spitler, Limitations of using uniform heat flux assumptions in sizing vertical borehole heat exchanger fields, in: Proceedings of Clima, Prague, Czech Republic, 2013.

[4] M. Cimmino, M. Bernier, F. Adams, A contribution towards the determination of g-functions using the finite line source, Appl. Therm. Eng. 51 (2013) 401–412, https://doi.org/10.1016/j.applthermaleng.2012.07.044.

[5] P. Eskilson, Thermal Analysis of Heat Extraction Boreholes. Ph.D. Thesis, University of Lund, Lund, Sweden, 1987.

[6] M. Cimmino, M. Bernier, A semi-analytical method to generate g-functions for geothermal bore fields, Int. J. Heat Mass Transf. 70 (2014) 641–665, https://doi.org/10.1016/j.ijheatmasstransfer.2013.11.037.

[7] P. Monzó, P. Mogensen, J. Acuña, F. Ruiz-Calvo, C. Montagud, A novel numerical approach for imposing a temperature boundary condition at the borehole wall in borehole fields, Geothermics 56 (2015) 35–44, https://doi.org/10.1016/j.geothermics.2015.03.003.

[8] C. Naldi, E. Zanchini, A new numerical method to determine isothermal g-functions of borehole heat exchanger fields, Geothermics 77 (2019) 278–287, https://doi.org/10.1016/j.geothermics.2018.10.007.

[9] M. Cimmino, The effects of borehole thermal resistances and fluid flow rate on the g-functions of geothermal bore fields, Int. J. Heat Mass Transf. 91 (2015) 1119–1127, https://doi.org/10.1016/j.ijheatmasstransfer.2015.08.041.

[10] M. Cimmino, Fast calculation of the g-functions of geothermal borehole fields using similarities in the evaluation of the finite line source solution, J. Build. Perform. Simul. 11 (2018) 655–668, https://doi.org/10.1080/19401493.2017.1423390.

[11] M. Cimmino, Semi-analytical method for g-function calculation of bore fields with series- and parallel-connected boreholes, Sci. Technol. Built Environ. 25 (2019) 1007–1022, https://doi.org/10.1080/23744731.2019.1622937.

[12] M. Cimmino, J.C. Cook, pygfunction 2.2: New features and improvements in accuracy and computational efficiency, Research Conference Proceedings, IGSHPA Annual Conference 2022, International Ground Source Heat Pump Association, 2022, pp. 45–52, https://doi.org/10.22488/okstate.22.000015.

[13] P. Monzó, A.R. Puttige, J. Acuña, P. Mogensen, A. Cazorla, J. Rodriguez, C. Montagud, F. Cerdeira, Numerical modeling of ground thermal response with borehole heat exchangers connected in parallel, Energ. Buildings 172 (2018) 371–384, https://doi.org/10.1016/j.enbuild.2018.04.057.

[14] E. Zanchini, C. Naldi, M. Dongellini, Dimensionless fluid-to-ground thermal response of single-line bore fields with isothermal fluid, Appl. Therm. Eng. 233 (2023) 121210, https://doi.org/10.1016/j.applthermaleng.2023.121210.

[15] E. Zanchini, F. Zanchini, A fast and accurate semi-analytical method to determine the thermal response of bore fields, Sci. Technol. Built Environ. 32 (2026) 112–129, https://doi.org/10.1080/23744731.2025.2518736.

[16] E. Zanchini, Comparison between conduction models and models including the energy balance along the flow, for the simulation of U-tube borehole heat exchangers, Appl. Therm. Eng. 257 (2024) 124311, https://doi.org/10.1016/j.applthermaleng.2024.124311.

[17] M. Cimmino, M. Basquens, A. Lazzarotto, Higher-order semi-analytical model for the simulation of geothermal boreholes, Int. J. Therm. Sci. 219 (2026) 110184, https://doi.org/10.1016/j.ijthermalsci.2025.110184.

[18] G. Hellström, Ground Heat Storage: Thermal Analyses of Duct Storage Systems—Theory. Doctoral Thesis, University of Lund, Lund, Sweden, 1991.

[19] S. Javed, J. Spitler, Accuracy of borehole thermal resistance calculation methods for grouted single U-tube ground heat exchangers, Appl. Energy 187 (2017) 790–806, https://doi.org/10.1016/j.apenergy.2016.11.079.

[20] J. Claesson, S. Javed, Explicit multipole formulas and thermal network models for calculating thermal resistances of double U-pipe borehole heat exchangers, Sci. Technol. Built Environ. 25 (2019) 980–992, https://doi.org/10.1080/23744731.2019.1620565.

[21] R.A. Beier, J.D. Spitler, Weighted average of inlet and outlet temperatures in borehole heat exchangers, Appl. Energy 174 (2016) 118–129, https://doi.org/10.1016/j.apenergy.2016.04.077.

[22] A. Jahanbin, C. Naldi, E. Zanchini, Relation between mean fluid temperature and outlet temperature for single U-tube boreholes, Energies 13 (2020) 828, https://doi.org/10.3390/en13040828.

[23] E. Zanchini, A. Jahanbin, Simple equations to evaluate the mean fluid temperature of double-U-tube borehole heat exchangers, Appl. Energy 231 (2018) 320–330, https://doi.org/10.1016/j.apenergy.2018.09.094.

[24] L. Lamarche, B. Beauchamp, New solutions for the short-time analysis of geothermal vertical boreholes, Int. J. Heat Mass Transf. 50 (2007) 1408–1419, https://doi.org/10.1016/j.ijheatmasstransfer.2006.09.007.

[25] G. Bandyopadhyay, M. Kulkarni, M. Mann, A new approach to modeling ground heat exchangers in the initial phase of heat flux build-up, ASHRAE Trans. 114 (2008) 428–439.

[26] G. Bandyopadhyay, W. Gosnold, M. Mann, Analytical and semi-analytical solutions for short-time transient response of ground heat exchangers, Energ. Buildings 40 (2008) 1816–1824, https://doi.org/10.1016/j.enbuild.2008.04.005.

[27] Y. Man, H. Yang, N. Diao, J. Liu, Z. Fang, A new model and analytical solutions for borehole and pile ground heat exchangers, Int. J. Heat Mass Transf. 53 (2010) 2593–2601, https://doi.org/10.1016/j.ijheatmasstransfer.2010.03.001.

[28] M. Li, A.C.K. Lai, Analytical model for short-time responses of ground heat exchangers with U-shaped tubes: model development and validation, Appl. Energy 104 (2013) 510–516, https://doi.org/10.1016/j.apenergy.2012.10.057.

[29] L. Lamarche, Short-time analysis of vertical boreholes, new analytic solutions and choice of equivalent radius, Int. J. Heat Mass Transf. 91 (2015) 800–807, https://doi.org/10.1016/j.ijheatmasstransfer.2015.07.135.

[30] R.A. Beier, Transient heat transfer in a U-tube borehole heat exchanger, Appl. Therm. Eng. 62 (2014) 256–266, https://doi.org/10.1016/j.applthermaleng.2013.09.014.

[31] R.A. Beier, Effects by geothermal gradient on thermal response tests for boreholes, Geothermics 121 (2024) 103029, https://doi.org/10.1016/j.geothermics.2024.103029.

[32] Z. Li, M. Zheng, Development of a numerical model for the simulation of vertical U-tube ground heat exchangers, Appl. Therm. Eng. 29 (2009) 920–924, https://doi.org/10.1016/j.applthermaleng.2008.04.024.

[33] G.A. Florides, P. Christodoulides, P. Pouloupatis, An analysis of heat flow through a borehole heat exchanger validated model, Appl. Energy 92 (2012) 523–533, https://doi.org/10.1016/j.apenergy.2011.11.064.

[34] T.Y. Ozudogru, C.G. Olgun, A. Senol, 3D numerical modeling of vertical geothermal heat exchangers, Geothermics 51 (2014) 312–324, https://doi.org/10.1016/j.geothermics.2014.02.005.

[35] X. Lei, X. Zheng, C. Duan, J. Ye, K. Liu, Three-dimensional numerical simulation of geothermal field of buried pipe group coupled with heat and permeable groundwater, Energies 12 (2019) 3698, https://doi.org/10.3390/en12193698.

[36] D. Marcotte, P. Pasquier, On the estimation of thermal resistance in borehole thermal conductivity test, Renew. Energy 33 (2008) 2407–2415, https://doi.org/10.1016/j.renene.2008.01.021.

[37] P. Pasquier, D. Marcotte, Joint use of quasi-3D response model and spectral method to simulate borehole heat exchanger, Geothermics 51 (2014) 281–299, https://doi.org/10.1016/j.geothermics.2014.02.001.

[38] M. De Carli, M. Tonon, A. Zarrella, R. Zecchin, A computational capacity resistance model (CaRM) for vertical ground-coupled heat exchangers, Renew. Energy 35 (2010) 1537–1550, https://doi.org/10.1016/j.renene.2009.11.034.

[39] A. Zarrella, M. Scarpa, M. De Carli, Short time step analysis of vertical ground-coupled heat exchangers: the approach of CaRM, Renew. Energy 36 (2011) 2357–2367, https://doi.org/10.1016/j.renene.2011.01.032.

[40] D. Bauer, W. Heidemann, H. Muller-Steinhagen, H.-J.G. Diersch, Thermal resistance and capacity models for borehole heat exchangers, Int. J. Energy Res. 35 (2011) 312–320, https://doi.org/10.1002/er.1689.

[41] D. Bauer, W. Heidemann, H.-J.G. Diersch, Transient 3D analysis of borehole heat exchanger modeling, Geothermics 40 (2011) 250–260, https://doi.org/10.1016/j.geothermics.2011.08.001.

[42] P. Pasquier, D. Marcotte, Short-term simulation of ground heat exchanger with an improved TRCM, Renew. Energy 46 (2012) 92–99, https://doi.org/10.1016/j.renene.2012.03.014.

[43] F. Ruiz-Calvo, M. De Rosa, J. Acuña, J.M. Corberán, C. Montagud, Experimental validation of a short-term borehole-to-ground (B2G) dynamic model, Appl. Energy 140 (2015) 210–223, https://doi.org/10.1016/j.apenergy.2014.12.002.

[44] P. Pasquier, A. Zarrella, R. Labib, Application of artificial neural networks to near-instant construction of short-term g-functions, Appl. Therm. Eng. 143 (2018) 910–921, https://doi.org/10.1016/j.applthermaleng.2018.07.137.

[45] P. Pasquier, D. Marcotte, Robust identification of volumetric heat capacity and analysis of thermal response tests by Bayesian inference with correlated residuals, Appl. Energy 261 (2020) 114394, https://doi.org/10.1016/j.apenergy.2019.114394.

[46] NIST, Chemistry WebBook. https://webbook.nist.gov/chemistry/fluid/, 2025.

[47] S.W. Churchill, Comprehensive correlating equations for heat, mass and momentum transfer in fully developed flow in smooth tubes, Ind. Eng. Chem. Fundam. 16 (1977) 109–116, https://doi.org/10.1021/i160061a021.

[48] P. Pasquier, P. Groleau, Comparaison des performances thermiques de puits géothermiques aménagés avec des conduits Versapipe HD et Geoperform, Research Report 08-1223-0083., Golder Associates, Montréal, Canada, 2009.